

# Caffeine Mediated Dissociation of a Potential Mutagen from DNA Mimetics, DNA and Cellular Nuclei: Ultrafast Spectroscopic Studies

Soma Banerjee, Samir Kumar Pal

**Abstract** – We present femtosecond to nanosecond-resolved studies of the dynamics of aqueous solvation within self-assembled dimeric structure of caffeine molecules. We have extended our studies in various temperatures in order to explore structural evolution of the self assemblies and consequently the dynamics of solvation in the interior of the dimer. Furthermore, we report a systematic investigation of caffeine induced dissociation of ethidium (Et) cation, a potential mutagen from nucleic acids and biomimetic systems. Time-resolved fluorescence studies are consistent with a mechanism where caffeine-Et complex formation in bulk solution drives the dissociation of DNA-bound Et. Temperature dependent picosecond resolved studies show the caffeine-Et complex to be stable over a wide range of temperature, within and beyond the normal physiological limit. A combination of NMR spectroscopy and DLS experiments allowed us to propose a molecular model of caffeine-Et complex. Caffeine induced extraction of Et from whole cells were also performed on squamous epithelial cells collected from the inner lining of the human mouth, A549 (lung carcinoma), A375 (human skin), RAW (macrophage) and Vero (African green monkey kidney epithelium) cell lines. Interestingly, the efficiency of caffeine in extracting Et has been found to be dependent on cell types. Our steady state and picosecond resolved spectroscopic studies on the detachment of Et from various biomimicking micelles of different charges reveal the specificity of caffeine molecule for carrying out such dissociation. The picosecond resolved Förster resonance energy transfer (FRET) studies between a DNA minor groove binder dye Hoeschst 33258 (H258, donor) and Et (acceptor) have been employed to investigate the alteration in their association in presence of caffeine in the molecular level. Finally, our fluorescence micrographs of epithelial cells validate the alteration of FRET efficiency between the donor and the acceptor due to the caffeine mediated release of the latter. Our results both in-vitro as well as ex-vivo provide important clues about efficiency and role of caffeine as a potential anti-mutagenic therapeutic agent. **Copyright** © 2012 Praise Worthy Prize S.r.l. - All rights reserved.

**Keywords:** Caffeine Dimer, Mutagen Dissociation, Femtosecond And Picosecond-Resolved Studies, Biomimetics, DNA, Cellular Nuclei, Ultrafast Förster Resonance Energy Transfer (FRET), Infelta-Tachiya Model

## Nomenclature

$C(t)$	Solvation correlation function	$\phi_s$	Specific volume
$r(t)$	Fluorescence anisotropy	$R_0$	Förster distance
$\tau_r$	Rotational relaxation time	$\kappa^2$	Orientation factor
$V_h$	Hydrodynamic volume	$n$	Refractive index
$\eta_m$	Microviscosity	$Q_D$	Quantum yield
$T$	Absolute temperature	$J(\lambda)$	Overlap integral
$\tau_i$	Fitted time parameters	$E$	Energy transfer efficiency
$\langle \tau \rangle$	Average time	$(E)$	Total energy
$A_i$	Relative weight of the time parameters	$E^*$	Activation energy
$d_H$	Hydrodynamic diameters	$r$	Distance between donor and acceptor
$k_B$	Boltzmann constant	$R$	Gas constant
$\beta$	Adiabatic compressibility	$\delta$	Chemical shift
$u$	Sound velocity	$K_M$ or $K$	Association/binding constant
$\rho$	Density	$\Delta G^0$	Free energy change
		$P_n^*$	Micelle containing n quencher molecules and one excited probe

$P_n$	Micelle containing n quencher molecules
$k_q$	Rate constant for quenching of an excited probe in a micelle containing one quencher molecule
$k_0$	Total decay constant of an excited probe in absence of quencher in micelle
$m$	Mean number of quenchers in a micelle
$[A]$	Concentration of quencher molecule in the aqueous phase
$k_+$	Rate constant for entry of a quencher molecule in a micelle
$k_-$	Rate constant for exit of a quencher molecule from a micelle containing one quencher molecule
$P^*(t)$	Total concentration of excited probes in a micelle at time t
$K_{eq}$	Equilibrium constant

## I. Introduction

Caffeine (1,3,7-trimethylxanthine) is in a class of molecules with conjugated planer ring systems that constitute the most widely distributed naturally occurring methylxanthines and regularly consumed by human beings from various dietary sources (e.g. coffee, tea, cola beverages, chocolates). Relatively higher consumption of the molecule due to abundance of methylxanthines (mainly caffeine) in human diets, has directed extensive research on the activity of the molecule in the cellular environments in the recent past [1]-[2]. It is clearly demonstrated that caffeine has multiplicity of effects on cells.

Particularly, it has been shown in a number of earlier studies that caffeine has variety of roles on the molecular recognition of DNA by intercalating drugs [2]-[3]. For example, when combined with a wide range of DNA-damaging agents (e.g. mitomycin C, cytophosphamide, cisplatinum, hydroxyl urea), caffeine enhances cell killing [4]-[5].

On the other hand another set of studies have indicated that caffeine can diminish the cytotoxic/cytostatic effects of doxorubicin, ethidium bromide [6]-[8] and reverses cytotoxic effect of the antitumor agent mitoxantrone, eilipticine and doxorubicin analogues [9]. The rational answer of the obvious question from the earlier studies that why does caffeine potentiate toxic effects in one group of drugs while having opposite effect on others, would be the specific molecular interaction of caffeine with individual drug molecule underlying in the “interceptor” action of caffeine [2]-[3]. For the physiological activity of the drugs in presence of caffeine another mechanism of action called “protector”, has been proposed, in which there is competition between caffeine and another aromatic drug for the binding sites on DNA [3],[9].

The activity of the molecule as mood altering substance is within the central nervous system where it acts as stimulant, perhaps by competitive blockage of endogenous adenosine at  $A_1$  and  $A_{2A}$  receptors [10].

From the brief survey of the earlier studies it is clear that caffeine can be used to host small ligands (drug) and deliver/remove the same in a specific site of adenosine receptor or DNA. In other words the molecular basis of use of the well known molecules as drug delivery/recovery system needs some attention. It is well known that specific interaction of a molecule/macromolecule with each other in aqueous solutions heavily depends on hydration of the molecule/macromolecules. In this regard caffeine should be considered as an interesting system because of the simultaneous presence of  $-CH_3$  and  $-OH$  groups on its structure (Scheme A).

The structure of the molecule limits the solubility in water because of the self association of the molecule by hydrophobic interaction and it is also responsible for complexation with other drug molecules in aqueous solutions. A detail NMR followed by molecular modelling studies confer that most stable self aggregation of caffeine is its dimeric form [11]. Earlier, spectroscopic and molecular modelling studies of caffeine complexes with other aromatic drugs reveal replacement of water molecules solvating the drugs by the more hydrophobic caffeine molecules [2]. The studies have also concluded that caffeine could make complex with drugs via  $\pi-\pi$  type of interaction.

It has to be noted that most of the DNA-binding drugs reveal charge transfer (CT) reaction upon  $\pi$ -stacking with DNA base pairs [12]-[13]. Thus the possibility of CT reaction of any drug upon complexation with caffeine molecule would be an interest for the molecular understanding of the interaction of caffeine with the drug. It is well established that the solvent relaxation time scales influence the dynamics of charge transfer reactions by exerting a time dependent dielectric friction.

In these cases the CT reaction rates are limited by the rate of solvent relaxation around the concerned molecule [14]-[15]. Therefore, exploration of the dynamics of solvent relaxation around caffeine upon complexation with other aromatic molecules along with the dynamics of CT of small molecules upon complexation with caffeine are of huge significance for better understanding of the biomolecular recognition of these xanthine alkaloids and are the motives of the present study.

Molecular recognition of DNA in *in vitro* condition by small ligands/drugs in presence of caffeine is well studied [1]-[2],[16].

Earlier, a set of studies have indicated that caffeine can diminish the cytotoxic/cytostatic effects of doxorubicin, ethidium (Et) bromide [8] and reverses cytotoxic effect of the antitumor agent mitoxantrone, eilipticine and doxorubicin analogues[9].

Spectroscopic studies on the de-intercalation of Et, a potential mutagen[17] from genomic DNA in solution at room temperature is also reported in the literature [18]. Such studies essentially intended to conclude the therapeutic use of caffeine in animal model. Therefore, a detail molecular picture of the de-intercalation mechanism and the universal application of such

xanthine alkaloids in the extraction of Et from the nucleus of various cell lines is of immense importance and is highlighted in our present report. Besides, the mechanism of de-intercalation both within and beyond the temperatures of physiological interest is also reported in the present study.

The molecular recognition of DNA by small ligands/drugs in presence of caffeine, a xanthine alkaloid, in aqueous solution is well known [1],[16],[19]. Earlier it is shown that the intercalation of novantrone, ellipticine, doxorubicin and ethidium bromide to DNA is significantly perturbed in presence of caffeine [2],[16],[20].

Other studies also reveal similar observations [18],[21]. A detail spectroscopic investigation from our laboratory [22] demonstrates the efficacy of caffeine in the removal of Et from synthetic self-complementary oligonucleotides and from different cell lines. The significant alteration of molecular recognition of DNA in caffeine solution has been concluded to depend on the 'protector' and 'interceptor' properties of caffeine [2],[9].

In the 'protector' mode of activity, there is a strong competition between caffeine and aromatic drug for the binding sites on DNA whereas in the 'interceptor' mode of its activity, caffeine forms hetero-complexes with a number of aromatic DNA intercalators, which account for the observed changes of biological activity of these drugs in the presence of caffeine. Sometimes, explanation of specific role of caffeine in the molecular recognition of DNA in physiological milieu becomes cumbersome [9].

In this regard small biomimetic systems including nanoscopic micelles [23] could serve as an efficient mimic for the biological membranes, macromolecules and are also useful in organizing the reactants at a molecular level [23]. For example, cationic hexadecyltrimethylammonium bromide (CTAB) micelles may act as a good mimic of histone protein [24], neutral (polar) Triton X-100 (TX-100) micelles may mimic a protein cavity [25] and anionic sodium dodecyl sulfate (SDS) micelles can serve as a good alternative of the DNA surface [26]-[27]. In this regard, our present study makes an attempt to explore the usage of nanoscopic micelles for the better understanding of caffeine mediated molecular recognition of DNA by small ligands/ drugs.

## II. Methodology

### II.1. NMR Measurements

<sup>1</sup>H-NMR experiments were performed on caffeine, TNS, Et and mixtures of caffeine-TNS and caffeine-Et (titrations) in aqueous phosphate buffer at pH 7.2 (Watergate solvent suppression) using a Bruker DRX 500 MHz spectrometer. <sup>1</sup>H-signals were assigned either by comparing with literature [28] or by performing TOCSY and NOESY/ROESY experiments using standard protocols.

### II.2. Steady State Measurements

Steady-state absorption, emission and Fourier transform infrared spectra (FTIR) were measured with Shimadzu Model UV-2450 spectrophotometer, Jobin Yvon Model Fluoromax-3 fluorimeter and JASCO FT/IR-6300 spectrometer (transmission mode) respectively.

Dynamic light scattering (DLS) measurements were done with Nano ZS Malvern instruments employing a 4 mW He-Ne laser ( $\lambda=632.8$  nm) equipped with a thermostatted sample chamber. The density and ultrasonic velocitometric studies are done with a DSA 5000 instrument from Anton Paar, with the measurement accuracy of density and sound velocity of  $5 \times 10^{-6}$  g cm<sup>-3</sup> and 0.5 ms<sup>-1</sup>, respectively.

### II.3. Details of Time Resolved, Dynamic Light Scattering (DLS) and Compressibility Measurements

All picosecond transients were measured by using commercially available (IBH, UK) picosecond-resolved time correlated single photon counting (TCSPC) setup (instrument response function (IRF) of 80 ps) using 375 and 409 nm excitation laser sources with temperature control setup from Julabo (Model: F32). Fluorescence from sample was detected by a photomultiplier after dispersing through a double grating monochromator. For all transients the polarizer in the emission side was adjusted to be at 54.7° (magic angle) with respect to the polarization axis of the excitation beam.

The temperature dependent femtosecond-resolved fluorescence is measured using a femtosecond upconversion setup (FOG 100, CDP) along with an indigenous temperature controller setup. The sample was excited at 409 nm (0.5 nJ per pulse), using the second harmonic of a mode-locked Ti-sapphire laser with an 80 MHz repetition rate (Tsunami, Spectra Physics), pumped by 10 W Millennia (Spectra Physics). The fundamental beam is frequency doubled in a nonlinear crystal (1mm BBO,  $\theta = 25^\circ$ ,  $\phi = 90^\circ$ ). The fluorescence emitted from the sample is up-converted in a nonlinear crystal (0.5 mm BBO,  $\theta = 10^\circ$ ,  $\phi = 90^\circ$ ) using a gate pulse of the fundamental beam.

The upconverted light is dispersed in a double monochromator and detected using photon counting electronics. A cross-correlation function obtained using the Raman scattering from water displayed a full width at half maximum (FWHM) of 165 fs. Upon excitation with a ultrafast laser pulse, a significant dipole moment is generated in the probe and hence the polar solvent molecules at  $t=0$  find themselves in a relatively high-energy configuration. Subsequently the solvent molecules begin to move and rearrange themselves to reach their new equilibrium positions. The shift in the probe's emission frequency (peak), which accompanies the solvent relaxation, gives a measure of the dynamics of solvation.

The observed fluorescence transients were fitted to a function comprising of the convolution of the instrument response function (IRF) with a sum of exponentials. For every sample solution, the fluorescence transients were measured as a function of the detected wavelength in the range of 560–720 nm for 4-(dicyanomethylene)-2-methyl-6-(p-dimethylaminostyryl) 4H-pyran (DCM) and 450–600 nm for coumarin 500 (C500).

The time-resolved emission spectra (TRES) were fitted with a lognormal shape function to estimate the spectrum maximum  $\nu(t)$ .

The temporal Stokes shift can be represented by the time dependence of the fit. By following the time-resolved emission, we constructed the solvation correlation function:

$$C(t) = [\nu(t) - \nu(\infty)] / [\nu(0) - \nu(\infty)] \quad (1)$$

where  $\nu(0)$ ,  $\nu(t)$  and  $\nu(\infty)$ , denote the observed emission peaks (in wavenumbers) at time 0, t and  $\infty$ , respectively.

For anisotropy measurements, emission polarization was adjusted to be parallel or perpendicular to that of the excitation and the anisotropy is defined as:

$$r(t) = [I_{para} - GI_{perp}] / [I_{para} + 2GI_{perp}] \quad (2)$$

where  $I_{para}$  and  $I_{perp}$  are the temporal emission intensities at parallel and perpendicular emission polarization with respect to vertical excitation polarization. The magnitude of  $G$ , the grating factor of the emission monochromator of the TCSPC system was found by longtime tail matching technique[29].

The temporal decay,  $r(t)$  has been fitted with single exponential function,  $r(t) = r_0 \exp(-t/\tau_r)$ , where  $r_0$  is the anisotropy at time  $t = 0$ . The rotational relaxation time,  $\tau_r$  of the fluorescent probe is related to the local microviscosity  $\eta_m$  experienced by the probe molecule through the Stokes–Einstein–Debye equation (SED) [30]–[31]:

$$\tau_r = \eta_m V_h / k_B T \quad (3)$$

where  $k_B$  is the Boltzmann constant,  $T$  is the temperature and  $V_h$  is the hydrodynamic volume of the probe. Using the  $\tau_r$  value in Eq. (3), the hydrodynamic volume of the probe is found out.

Furthermore, the rotational time constants were recalculated using the reported method for fluorescence anisotropy analysis [32]. In this analysis the basic equations used to fit the parallel ( $I_{para}$ ) and perpendicular ( $I_{perp}$ ) components of the emission transients are:

$$I_{para} = \frac{1}{3} F(t) [1 + 2r(t)] \quad (4a)$$

$$I_{perp} = \frac{1}{3} F(t) [1 - r(t)] \quad (4b)$$

where  $F(t)$  is the pure excited state population decay, free of anisotropy effect; can be written as:

$$F(t) = F_0 \exp(-t/\tau_F)$$

$\tau_F$  being the average lifetime of the fluorophore estimated from the reconvolution fitting analysis of the fluorescence decay taken at magic angle  $54.7^\circ$ .  $r(t)$  is the anisotropy decay at time t and is given by:

$$r(t) = r_0 \exp(-t/\tau_r) \quad (5)$$

where  $\tau_r$  is the rotational time constant and  $r_0$  is the anisotropy at time  $t = 0$ . Substituting  $r(t)$  and  $F(t)$  into Eq. (4) yields:

$$I_{para} = \frac{1}{3} F_0 \exp(-t/\tau_F) + \frac{2}{3} F_0 r_0 \exp\left(-t/\frac{\tau_F \tau_r}{\tau_F + \tau_r}\right) \quad (6a)$$

$$I_{perp} = \frac{1}{3} F_0 \exp(-t/\tau_F) - \frac{1}{3} F_0 r_0 \exp\left(-t/\frac{\tau_F \tau_r}{\tau_F + \tau_r}\right) \quad (6b)$$

Now both  $I_{para}$  and  $I_{perp}$  decays can be fitted bi-exponentially as:

$$I_{para} = A_1 \exp\left(\frac{-t}{\tau_1}\right) + A_2 \exp\left(\frac{-t}{\tau_2}\right) \quad (7a)$$

$$I_{perp} = A'_1 \exp\left(\frac{-t}{\tau_1}\right) + A'_2 \exp\left(\frac{-t}{\tau_2}\right) \quad (7b)$$

where  $\tau_i$  represents fitted time parameters and  $A_i$  its relative weight.

Comparing Eq. (6) and (7) one can find out the values of  $\tau_r$  and  $r_0$ . All DLS measurements were taken at  $173^\circ$  scattering angle. The scattering intensity data were processed using the instrumental software to obtain the hydrodynamic diameter ( $d_H$ ) and the size distribution of the scatterer in each sample. The instrument measures the time-dependent fluctuation in intensity of light scattered from the particles in solution at a fixed scattering angle.

Hydrodynamic diameters ( $d_H$ ) of the particles were estimated from the intensity auto correlation function of the time-dependent fluctuation in intensity.  $d_H$  is defined as:

$$d_H = k_B T / 3\pi\eta D \quad (8)$$

where  $k_B$  = Boltzmann constant,  $T$  = absolute temperature,  $\eta$  = viscosity and  $D$  = translational diffusion coefficient. In a typical size distribution graph from the DLS

measurement, X-axis shows a distribution of size classes in nm, while the Y-axis shows the relative intensity of the scattered light.

Adiabatic compressibility ( $\beta$ ) of caffeine solution was determined by measuring the density of caffeine solution ( $\rho$ ) and the sound velocity ( $u$ ) and applying Laplace's equation [33]:

$$\beta = 1/\rho u^2 \quad (9)$$

The apparent specific volume ( $\phi_v$ ) is given by:

$$\phi_v = 1/\rho_0 + (\rho_0 - \rho)/c\rho_0 \quad (10)$$

where,  $\rho_0$  is the density of water and  $c$  is the concentration of caffeine solution.

#### II.4. Molecular Modeling Studies

For the molecular modeling studies, we have followed the procedure as reported earlier for the calculation of caffeine hetero-dimer with a number of DNA-intercalating dyes [2]. We have used commercially available ChemBio3D (from CambridgeSoft<sup>TM</sup>) ultra software.

The force field employed for these calculations is MM2 with default parameters provided with the software. Conjugate gradient methods were used to search for geometry-optimized structures with a convergence criterion of 0.0001 kcal/Å.

The minimized energy values of the various complexes as investigated in the present study (caffeine-caffeine, caffeine-DCM, caffeine-C500 and caffeine-TNS) are obtained by first geometry optimizing each component of the complex in vacuum. These geometry-optimized components were then brought together in a face to face orientation and to within van der Waals radii and re-optimized. Relative binding energies were determined by subtracting the sum of the geometry-optimized energies of the isolated components from the total energy obtained for the geometry-optimized complex. In general the lowest energy conformation is that in which the caffeine is oriented directly over the conjugated rings of the various dyes with an average face to face distance of 3.5 Å.

It must be pointed out that the orientation of the caffeine relative to the dyes in the geometry-optimized complexes is not unique. For example, small displacement (~1 Å) and rotation of the caffeine by 180 degree relative to a dye ring system does not significantly alter the relative binding energy. The relative binding energies derived from molecular mechanics methods can be further deconvoluted into individual components that makeup the total energy.

However, in our present study we like to be limited in the overall stabilization energy of the complexes as shown in Table I. However, we have recognized that the dominant force in the formation of such complexes appears to be van der Waals interactions resulting in

maximal ring overlap between the two molecules of the complexes.

#### II.5. Fluorescence Microscopy Studies

Fluorescence micrographs were taken using Olympus BX51 fluorescence microscope connected with DP72 microscope digital camera. Olympus fluorescence microscope is equipped with various sets of fluorescence mirror unit combined with appropriate filters which are variable depending on wavelengths. The fluorescence mirror unit which matches the fluorochrome in use was selected. Cells were irradiated under UV light at 360 nm continuously for 800 seconds. All the images were taken under 50X magnification. The micrographs were analyzed with analySIS Five image analysis software provided with the microscope. The software was used to measure the intensity of red, green and blue component in each micrograph.

#### II.6. Förster Resonance Energy Transfer (FRET) Studies

In order to estimate the Förster resonance energy transfer (FRET) efficiency of the donor Hoeschst 33258 (H258) to the acceptor Ethidium (Et) and hence, to determine distances of donor-acceptor ( $D-A$ ) pairs, we have followed the methodology described in chapter 13 of ref[34]. The Förster distance ( $R_0$ ) is given by:

$$R_0 = 0.211 \left[ \kappa^2 n^{-4} Q_D J(\lambda) \right]^{1/6} \quad (11)$$

(in Å)

where ( $\kappa^2$ ) is a factor describing the relative orientation in space of the transition dipoles of the donor and acceptor.

The value of the orientation factor ( $\kappa^2$ ) is calculated from the equation:

$$\kappa^2 = (\cos \theta_T - 3 \cos \theta_D - \cos \theta_A) \quad (12)$$

where  $\theta_T$  is the angle between the emission transition dipole of the donor and absorption transition dipole of the acceptor and  $\theta_D$  and  $\theta_A$  are the angles between these dipoles and the vector joining the donor and acceptor [34].

In the micellar system, the donor and acceptor molecules can be bound simultaneously without any restriction on the relative orientation of their transition dipole moments. Thus, the orientation parameter ( $\kappa^2$ ) can be taken as 0.667 [34].

Moreover, since the sixth root is taken to calculate the distance, variation of  $\kappa^2$  from the value for random orientation ( $\kappa^2 = 2/3$ ) to that for parallel dipolar orientation ( $\kappa^2 = 1$ ) or to that for head-to-tail parallel transition dipoles ( $\kappa^2 = 4$ ) the calculated distance can be in error by no more than 35% [34]. The refractive index ( $n$ ) of the medium is assumed to be 1.4.  $Q_D$ , the quantum

yield of the donor H258 in the absence of acceptor Et in SDS micelles is 0.54 and 0.3 in absence [35] and presence of caffeine, respectively.  $J(\lambda)$ , the overlap integral, which expresses the degree of spectral overlap between the donor H258 emission and the acceptor Et absorption, is given by:

$$J(\lambda) = \frac{\int_0^{\infty} F_D(\lambda) \varepsilon(\lambda) \lambda^4 d(\lambda)}{\int_0^{\infty} F_D(\lambda) d(\lambda)} \quad (13)$$

where  $F_D(\lambda)$  is the fluorescence intensity of the donor in the wavelength range of  $\lambda$  to  $\lambda + d\lambda$  and is dimensionless.  $\varepsilon(\lambda)$  is the extinction coefficient (in  $M^{-1} \text{ cm}^{-1}$ ) of the acceptor at  $\lambda$ . If  $\lambda$  is in nm, then  $J(\lambda)$  is in units of  $M^{-1} \text{ cm}^{-1} \text{ nm}^4$ .

Once the value of  $R_0$  is known, the D-A distance ( $r$ ) can easily be calculated using the formula:

$$r^6 = \left[ R_0^6 (1-E) \right] / E \quad (14)$$

here,  $E$  is the efficiency of energy transfer. The efficiency ( $E$ ) is calculated from the lifetimes of the donor in the absence and presence of acceptors ( $\tau_D$  and  $\tau_{DA}$ ):

$$E = 1 - \frac{\tau_{DA}}{\tau_D} \quad (15)$$

The longer lifetime component in the decay of D-A pair that resembles the decay component of the donor alone is due to less than 100% labelling by acceptor[34] and has not been considered while calculating  $\tau_{DA}$ .

In order to prevent homomolecular energy transfer between donor molecules and to ensure efficient energy transfer between the donor and acceptor, the concentration of the donor molecules is kept low (0.2  $\mu\text{M}$ ) while that of the acceptor molecules is 155  $\mu\text{M}$  which is comparable to the micellar concentration of 194  $\mu\text{M}$  (surfactant SDS concentration being 20 mM).

### III. Results and Discussions

#### III.1. Probing the Interior of Self-Assembled Caffeine Dimer at Various Temperatures

In the present section we have explored the structure of caffeine aggregation by DLS and FTIR techniques. Temperature dependent DLS studies followed by densimetric & sonometric measurements of the caffeine molecules in aqueous solutions explore the structural evolution of caffeine self-aggregation with temperature.

These studies are of particular interest as caffeine is consumed as low and high temperature beverages. Here we have also explored the details of the complexation (solubilisation) of caffeine with a hydrophobic (completely insoluble in water) model probe ligand 4-(dicyanomethylene)-2-methyl-6-(p-dimethylaminostyryl)

4H-pyran (DCM), a well known fluorescent reporter for the relaxation of solvent molecules, in water.

Our molecular modeling on the complexation of DCM with caffeine molecules reveals that two caffeine molecules make stack geometry in order to encapsulate DCM inside the dimeric structure (Scheme A). We have measured solvation response of water molecules around the probe DCM at 80°C in the host caffeine dimer with limited number of water molecules and compared the time scales of the solvation with bulk water at elevated temperature. In order to establish the general nature of the solvation dynamics (independent of probe), we have used another well known solvation probe coumarin 500 (C500), where similar complexation geometry with the caffeine molecules has been modelled. Polarization gated fluorescence upconversion and time correlated single photon counting (TCSPC) have been employed to confirm the geometrical restriction of the probes under investigation.

In order to investigate the consequence of the slower solvation of water molecules and restricted geometry on the photo-induced charge transfer reaction, we have studied twisted intramolecular charge transfer (TICT) of the probe 2-(p-toluidino) naphthalene-6-sulfonate (TNS) in the dimer at various temperatures. Our detail experimental evidences clearly establish caffeine dimer as an excellent host of small molecules, which could be useful to the further research on the application of the well consumed beverage as a potential carrier of drug for targeted delivery system[36].

#### III.1.1. Characterization of Caffeine Dimer in Aqueous Solution

As shown in Table I and Scheme A, our molecular modeling studies reveal a stable stacked dimer of caffeine molecules with stabilization energy of  $\sim 10$  kcal/mole. Our estimated value of the stabilization energy is close proximity of the reported value of 39.9 kJ/mole ( $\sim 9.5$  kcal/mole) from the molecular modeling (using Gaussian package) and X-ray crystallographic studies [37].

As a direct evidence of the formation of caffeine aggregates, we perform temperature and concentration dependent DLS measurements of aqueous caffeine solution (Fig. 1). High concentration of caffeine in aqueous solution (0.9 M) is reached at a high temperature of 80°C. We observe a hydrodynamic diameter of  $\sim 1$  nm with no signature of any larger sized aggregates, and this feature does not show any significant change with the variation of temperature from 5° to 80°C (Fig. 1). A similar size distribution is observed when the concentration of the solution is increased from 45 mM to 900 mM.

Since the radius of caffeine molecule is 3.76 Å [38] the observed hydrodynamic diameter of  $\sim 1$  nm in caffeine solution does not support the probability of formation of large caffeine aggregate over the studied temperature and concentration range.

TABLE I  
SUMMARY OF MOLECULAR MODELING CAFFEINE-DYE COMPLEXES:  
ERROR  $\pm 7\%$

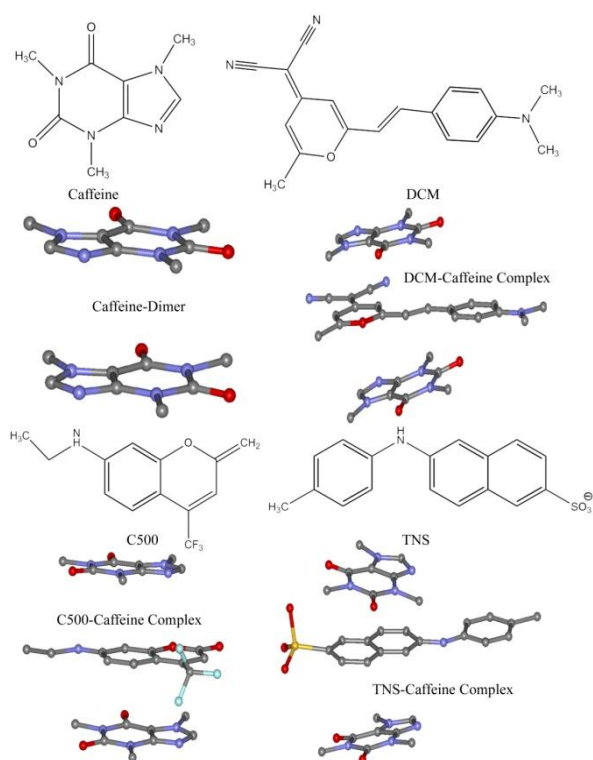
Complex	Total Energy* (E) (kcal/mole)	Complex Energy# (kcal/mole)	$\Delta E^\ddagger$ (kcal/mole)
CAF-CAF	55.56	45.53	-10.03
CAF-DCM	51.91	40.7	-11.21
CAF-DCM-CAF	79.69	57.48	-22.21
CAF-C500	46.89	36.18	-10.71
CAF-C500-CAF	74.67	52.91	-21.68
CAF-TNS (Phenyl side)	28.58	20.85	-7.73
CAF-TNS (Naphthalene side)	28.58	18.41	-17.32
CAF-TNS-CAF (Both CAF are in Phenyl side)	56.36	39.04	-17.32
CAF-TNS-CAF (One CAF is in Phenyl side another is in Naphthalene side)	56.36	29.29	-27.07
CAF-TNS-CAF (Both CAF are in Naphthalene side)	56.36	28.07	-28.29

CAF=Caffeine

\*Mathematical sum of energy (E) for each molecule in the complex.

#Total energy calculated for various configurations of the molecular complexes.

‡Difference between mathematical sum of energies of individual molecules and calculated energies of each complex



**Scheme A.** The molecular structure of caffeine and the fluorescent probes DCM, C500, and TNS along with their complexes with caffeine dimer. (Reprinted with permission from ref.[36]. Copyright 2011, Springer Science + Business media)

To reconfirm the self-association of caffeine, we also carry out FTIR and densimetric measurements, and the results are shown in Figs. 2. Fig. 2(a) shows the FTIR transmittance spectra for caffeine at different concentrations. The spectrum is in good agreement with previously reported studies [11],[39]. The major information of caffeine stretching is confined in the 1700-1640  $\text{cm}^{-1}$  region in which two major peaks are obtained, one in the 1692-1700  $\text{cm}^{-1}$  region (band 1) due to the stretching of the isolated carbonyl, and the other one in the 1641-1647  $\text{cm}^{-1}$  region (band 2), due to the stretching of the conjugated carbonyl.

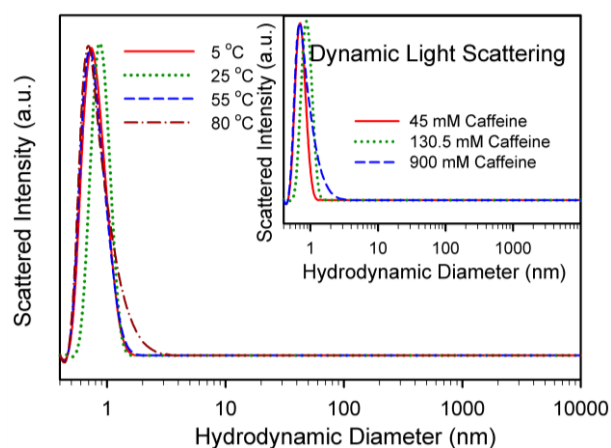


Fig. 1. Hydrodynamic diameter (as obtained from DLS measurements) of 130.5 mM aqueous caffeine solution at three different temperatures.

DLS measurements of caffeine solution with three different concentrations at 25 °C are shown in the inset. (Reprinted with permission from ref.[36]. Copyright 2011, Springer Science + Business media)

Less intense bands are produced in the 1570  $\text{cm}^{-1}$  region due to  $C=N$  and  $C=C$  stretching vibrations of the purine ring. As can be observed from Fig. 2(a), negligible change in the peak position of band 1 and band 2 occurs with increase in the caffeine concentration indicating the presence of no higher order aggregates [39]. It can also be noted here that in case of stacked dimers of caffeine, full hydration of the carbonyl group is hindered due to steric hindrance, which may in turn cause a wavenumber shift of  $C=O$  stretching mode by  $\sim 20 \text{ cm}^{-1}$ . Thus the present result concludes the presence of the dimers with relatively lower hydration of caffeine which corroborates the compressibility studies (see later).

Our observation complies with earlier studies [11] involving theoretical Monte Carlo simulation, FTIR and NMR spectroscopies revealing that caffeine molecules associate to form stacked dimers in water that are energetically more favourable than monomers.

In order to understand the nature of hydration in caffeine aggregates, we perform density and sound velocity measurements and the results are depicted in

Fig. 2(b) and Table II. As observed from Fig. 2(b) and Table II, the apparent molar volume ( $\phi_v$ ) decreases with increasing concentration of caffeine. However, the concentration vs.  $\phi_v$  plot does not produce a good linear fit generally observed for many small ionic compounds.

We attempt to fit the curves in a polynomial of concentration (c):

$$\phi_v = \phi_v^0 + \sum_{i=1}^n S_{v_i} c^i \quad (16)$$

and found the  $\phi_v^0$  values as  $8.192 \times 10^{-4}$ ,  $8.326 \times 10^{-4}$ ,  $8.478 \times 10^{-4}$  and  $8.602 \times 10^{-4} \text{ m}^3 \text{ kg}^{-1}$  at 10, 20, 30 and  $40^\circ\text{C}$ , respectively, which are relatively large compared to the small solute molecules but are considerably close to the values reported for large organic molecules [40].

The departure from linear behavior of caffeine molecules strongly suggests its association behavior in aqueous solution as has been found from the FTIR and DLS measurements.

The ultrasonic velocity and adiabatic compressibility ( $\beta$ ) decreases with increasing caffeine concentration (Fig. 2(c) and Table II), a trend similar to that observed for electrolyte solutes [33], [41] in which increasing electrolyte concentration makes more water molecules to electrorestrict resulting in a decrease in the fraction of bulk water in the solution. This is unusual for a neutral molecule like caffeine to show a negative  $d\beta/dc$  slope.

However, the slope  $d\beta/dc$  is very small for caffeine indicating a low hydration number associated with caffeine, similar to that reported earlier [38].

It is known that  $d\beta/dc$  is negative for structured water while it is positive for the non-structured one. A small negative value of  $d\beta/dc$  thus indicates that the hydration water molecules are rather weakly attached to the caffeine dimers.

### III.1.2. Complexation of Caffeine Dimer with DCM: Dynamics of Solvation

The molecular modeling studies on the caffeine-DCM complexation (Table I, Scheme A) confirm that ternary complex of two molecules of caffeine and one DCM molecule (22.21 kcal/mole) is much stable compared to the hetero dimer of caffeine and DCM (11.21 kcal/mole), which has almost similar stabilization energy of caffeine dimer. DCM, being completely insoluble in water, can be solubilized only within some self organized assemblies in aqueous solution [42].

We monitor the solubility of DCM in caffeine solution as a function of caffeine concentration by measuring the optical density of DCM at the absorption maximum (Fig. 3(a)). From the plot it is evident that the solubility of DCM increases linearly beyond 40 mM, and at 140 mM caffeine concentration  $1\mu\text{M}$  DCM can be solubilized in the solution. Therefore it can be concluded that  $1.4 \times 10^5$  molecules of caffeine are involved to solubilize 1

molecule of DCM. Two different conditions can give rise to such result. Firstly, if caffeine forms a large aggregate with critical concentration of 40 mM and secondly, if there is a hetero-association of caffeine with DCM at high caffeine concentration.

The probability of caffeine forming large aggregate with critical concentration of 40 mM can be ruled out from the DLS experimental result where we found no signature of aggregate formation in the solution of 140 mM caffeine with dissolved DCM (data not shown).

TABLE II  
APPARENT MOLAR VOLUME ( $\phi_v$ ) AND ADIABATIC COMPRESSIBILITY ( $\beta$ ) OF CAFFEINE SOLUTIONS AT DIFFERENT TEMPERATURES.  
ERROR  $\pm 7\%$

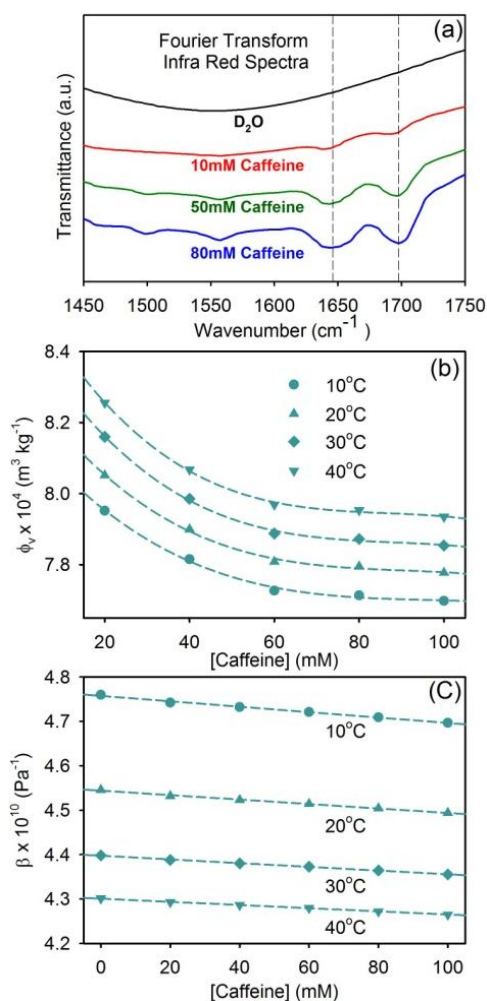
[Caffeine] mM	Density ( $\text{g cm}^{-3}$ )	Sound velocity ( $\text{m s}^{-1}$ )	$\phi_v \times 10^4$ ( $\text{m}^3 \text{ kg}^{-1}$ )	$\beta \times 10^{10}$ ( $\text{Pa}^{-1}$ )
<b>Temp. = 10°C</b>				
0	1.000841	1448.87	-	4.7596
20	1.001634	1450.99	7.9516	4.7420
40	1.002533	1451.87	7.8152	4.7320
60	1.003482	1452.88	7.7269	4.7209
80	1.004383	1454.08	7.7136	4.7089
100	1.005299	1455.36	7.6979	4.6963
<b>Temp. = 20°C</b>				
0	0.999320	1483.72	-	4.5456
20	1.000079	1485.43	8.0513	4.5317
40	1.000956	1486.20	7.8992	4.5230
60	1.00188	1486.98	7.8082	4.5141
80	1.002754	1487.98	7.7949	4.5041
100	1.003647	1489.04	7.7771	4.4937
<b>Temp. = 30°C</b>				
0	0.996749	1510.31	-	4.3878
20	0.997474	1511.56	8.1598	4.3802
40	0.998334	1512.21	7.9855	4.3726
60	0.999240	1512.84	7.8878	4.3642
80	1.000094	1513.64	7.8725	4.3553
100	1.000966	1514.54	7.8540	4.3878
<b>Temp. = 40°C</b>				
0	0.993308	1529.91	-	4.3011
20	0.994007	1530.85	8.2555	4.2928
40	0.994851	1531.36	8.0676	4.2863
60	0.995737	1531.87	7.9687	4.2796
80	0.996571	1532.61	7.9529	4.2719
100	0.997422	1533.23	7.9346	4.2648

The relatively high solubility of DCM in caffeine solution compared to its water-insolubility strongly suggests the self-association of caffeine providing a hydrophobic environment wherein DCM can be solubilized.

Since DCM has been found to be completely insoluble in aqueous solution of sucrose, urea and guanidine hydrochloride even at a high concentration of 6M each, the result clearly signifies the entrapment of the probe within caffeine dimers rather aqueous solution with perturbed hydrogen bonding networks.

Fig. 3(b) shows the relative emission intensity of DCM in aqueous caffeine solution as a function of caffeine concentration and the inset shows the corresponding emission spectra.

The Figure shows significant increase in the emission intensity beyond 40 mM caffeine concentration which corroborates the absorption results (Fig. 3(a)).

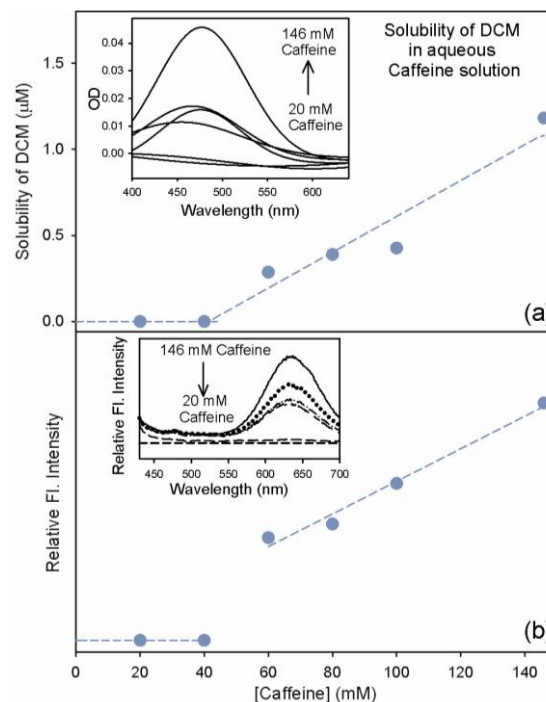


Figs. 2. (a) FTIR spectra of caffeine solutions at different concentrations (10 mM, 50 mM and 80 mM). The broken line indicate C=O stretch frequencies. (b) Partial molar volume of caffeine as a function of caffeine concentration in solution at different temperatures. The broken lines are polynomial fits. (c) Adiabatic compressibility of aqueous caffeine solution as a function of caffeine concentration at different temperatures. The broken lines are linear fits. (Reprinted with permission from ref.[36]. Copyright 2011, Springer Science + Business media)

In aqueous solution of caffeine, the only probable location of hydrophobic DCM is some hydrophobic pocket. Thus the increase in emission intensity is exclusively due to the relocation of DCM molecule in the hydrophobic environment of low order caffeine aggregates.

Earlier studies show that the emission maximum of DCM is produced at 636 nm in micelles [43].

In microemulsion system the DCM emission peak is blue shifted compared to that in micelles and suffers a progressive red shift from 570 nm to 625 nm with increasing water content of the microemulsion [44]. The present observation of the peak at ~635 nm reveals a hydrophobic environment around DCM molecule which is more or less comparable to that in micelles and large microemulsions, which in turn is close to that obtained in highly polar solvents (like methanol, ethyl acetate, acetonitrile) [45]-[46].



Figs. 3. (a) Solubility of DCM at different caffeine concentrations as obtained from absorption measurements. The corresponding absorption spectra are shown in the inset. (b) Relative fluorescence intensity of DCM at its emission maxima in various caffeine concentrations. The inset shows the corresponding fluorescence spectra. (Reprinted with permission from ref.[36]. Copyright 2011, Springer Science + Business media)

We now focus on the dynamics of water molecules (solvation) associated with the caffeine dimers. Figure 4(a) depicts the picosecond resolved fluorescence transients of DCM in 146 mM caffeine aqueous solution at 25°C.

As observed from the Figure, the fluorescence transients at the blue end (580 nm), peak (630 nm) and at the red end (690 nm) do not differ considerably and there is no rise component in the red end, a situation markedly different from the other self-aggregated systems like micelles [43]. The transients can be fitted biexponentially with time components of ~350 ps and ~800 ps, resulting in an average lifetime of ~750 ps. It has to be noted that the convolution cis-trans isomerization dynamics of the probe DCM, [47] which is evident in the nonpolar solvents could be of potential concern in the solvation time scales. However, later works on the exploration of solvation dynamics using the probe DCM have accounted a consequent strong coupling between the locally excited (LE) and charge transfer (CT) states [48] (~300 fs) in bulk polar solvents rather the isomerization dynamics [49].

The absence of considerable difference in the wavelength dependent fluorescence transients rules out the existence of any slow solvation dynamics, which is typical for aggregates like micelles. This result identifies the hydrated water molecules to be loosely bound to the caffeine dimers as has previously been inferred from compressibility measurements.

Identical result is obtained at 80°C using a high caffeine concentration of 900 mM (data not shown), concluding that the nature of aggregation and hydration dynamics does not change with temperature as has been observed from the DLS measurements (Figure 1). In order to study the geometrical restriction on the encapsulated DCM, in other word to investigate the change in the overall hydrodynamic diameter of the caffeine-DCM complex in aqueous solution, we measure the time resolved fluorescence anisotropy of DCM at 25°C in 146 mM caffeine solution (Fig. 4(a), inset). The transient can be fitted single exponentially with a time constant of 0.31 ns which is almost similar to that in ethanol (0.27 ns) but faster than that in micelles [43], thus corroborates with the other experimental results ruling out the possibility of formation of higher order aggregates of caffeine in solution. The hydrodynamic volume of the probe is found to be  $1.11 \times 10^{-27} \text{ m}^3$  in ethanol and  $1.39 \times 10^{-27} \text{ m}^3$  in caffeine solution. The slightly higher hydrodynamic volume of the probe in the latter system assures the interaction of the probe with the caffeine molecules and simultaneously confirms the absence of higher order aggregates of caffeine in aqueous solution. To have a detailed understanding of the microenvironment around DCM at higher temperatures, we measure temperature dependence of the rotational relaxation dynamics. It is observed that  $\tau_r$  decreases gradually with increasing temperature indicating that the probe experiences less rotational hindrance at higher temperature (Table III).

The ease of rotation with increasing temperature can be related to an activation energy barrier crossing model and the microviscosity changes with temperature following the relation [50]:

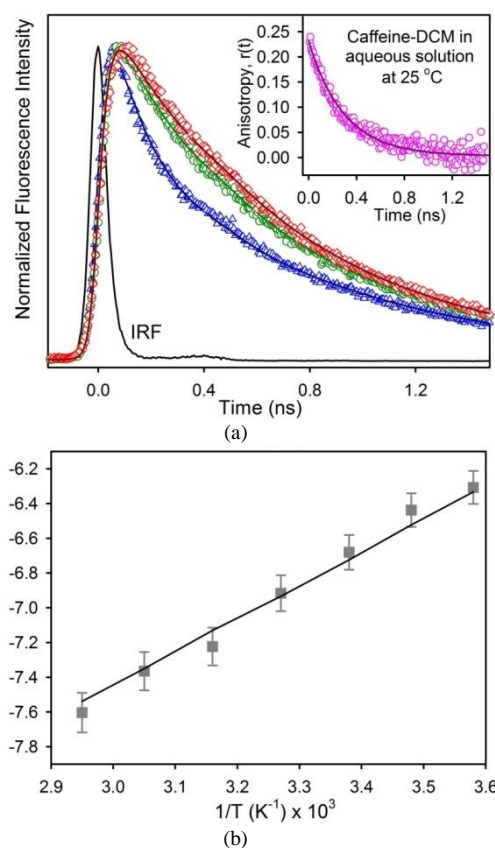
$$\eta_m = \eta_m^0 \exp\left(\frac{-E^*}{RT}\right) \quad (17)$$

where  $E^*$  is the activation energy for the viscous flow.

The plot of  $\ln(\eta_m)$  against  $1/T$  (Fig. 4(b)) can be linearly fitted within an experimental error of  $\pm 1.5\%$ . Aqueous micellar solutions show a relatively large deviation from linear behavior ( $\pm 10\%$ ) of temperature dependent microviscosity, which can be explained by the presence of higher order aggregates in the solution in the close proximity of Kraft temperature [50].

The relatively strong linear behavior in the caffeine system confirms the low order self-associated stacked caffeine dimers. The obtained  $E^*$  value of  $3.7 \text{ kcal mol}^{-1}$  is comparable to that of the bulk water ( $3.9 \text{ kcal mol}^{-1}$ ), but considerably smaller than micellar systems [50].

To ascertain the dynamical states of water molecules associated with the caffeine dimer, we measure the femtosecond resolved fluorescence spectra of DCM in caffeine solution. In order to ensure high signal to noise ratio, we measure the transients at 80°C where the caffeine solubility is high enough (900 mM) to provide high signal from the fluorophore.



Figs. 4. (a) Picosecond resolved fluorescence transients of DCM in 146 mM caffeine solution at 25°C shown at three characteristic wavelengths of 580 nm (blue triangles), 630 nm (green circles) and 690 nm (red diamonds). The Instrument response function (IRF) is shown for comparison (Excitation at 409 nm). The solid lines are exponential fittings. The insets shows time resolved anisotropy,  $r(t)$  of DCM in the corresponding solution. The solid line is exponential fit. (b) Plot of  $\ln(\eta_m)$  against  $1/T$  for caffeine solution. The solid line is a linear fit. (Reprinted with permission from ref.[36]. Copyright 2011, Springer Science + Business media)

TABLE III  
TEMPERATURE-DEPENDENT ROTATIONAL RELAXATION TIME  
CONSTANTS ( $\tau_r$ ) OF DCM IN 146 MM AQUEOUS CAFFEINE SOLUTION  
( $R_0$  DEFINES ANISOTROPY AT TIME  $T=0$ ). ERROR  $\pm 7\%$

Temperature (°C)	$r_0$	$\tau_r$ (ps)
06	0.25	484
14	0.24	413
23	0.25	314
33	0.23	240
43	0.23	171
55	0.20	143
66	0.20	109

We have also checked the stability of the probe at such elevated temperature in our system and found it to be highly stable.

Fig. 5(a) depicts the femtosecond resolved transients in the blue end (560 nm), peak (620 nm) and in the red end (700 nm). As can be observed from the Figure, the transient in the blue end can be fitted triexponentially with three decay components of 0.46 ps (86%), 22.7 ps (11%) and 519 ps (3%). On the other hand, the red end transient exhibits a distinct rise component of 0.94 ps with a decay component of 510 ps. This is a clear

indication of the solvation of the dye and we construct the TRES (see Fig. 5(b), inset) as per the procedure described in the methodology. From the time dependent Stokes shift we measure the solvent correlation function,  $C(t)$  and plot it against time (Fig. 5(b)). The curve is well fitted biexponentially with time constants of 0.6 ps (82%) and 5.85 ps (18%) (Table IV) with a considerable Stokes shift of  $800\text{ cm}^{-1}$ . It should be noted here that we miss a considerable fraction of Stokes shift due to our limited instrumental resolution, and we determined the loss in the dynamic Stokes shift using the procedure developed by Fee and Maroncelli [51], where  $\nu(0)$  can be calculated by the following equation:

$$\nu_{em}^p(0) = \nu_{abs}^p - [\nu_{abs}^{np} - \nu_{em}^{np}] \quad (18)$$

where  $\nu_{abs}^p$ ,  $\nu_{abs}^{np}$ , and  $\nu_{em}^{np}$  are the absorption peak in polar solvent, absorption peak in nonpolar solvent, and emission peak in nonpolar solvent, respectively. In the present study, we use dioxane as the nonpolar solvent with absorption and emission maxima of DCM at 455 and 554 nm, respectively. Aqueous solution of caffeine is used as the polar solvent in which DCM produces an absorption peak at 480 nm. We calculate a 34% loss in the dynamical Stokes shift within the experimental time resolution.

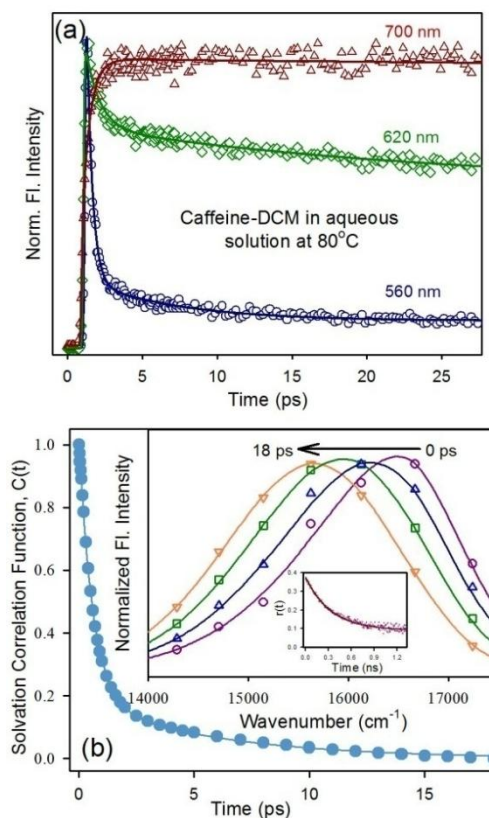
The observed  $C(t)$  decay is much slower than that of the pure water [52] (126 fs (20%) and 880 fs (35%)) wherein about half of the solvation process occurs in a time scale of experimental time resolution of 30 fs. A previous femtosecond-resolved study from our group shows that the solvation time scale of C500 in water is 0.3 and 0.7 ps at room temperature and it reduces to 0.3 ps at 55°C.

In presence of a large ion like guanidium hydrochloride the process becomes slower with time constants of 0.5 and 2.1 ps at room temperature and 0.8 ps at 55°C. All these time scales are however, faster than those observed for caffeine solutions even at elevated temperature confirming the structured nature of the hydrated water molecules in caffeine solution with respect to an ionic solution. On the other hand these time scales are rather comparable [53] or faster [54] in reverse micelles or micelles [43] confirming our finding that caffeine is aggregated as dimers in aqueous solution and with a rather weakly structured water network around it.

The smaller inset inside Fig. 5(b) inset shows fluorescence anisotropy of DCM at 80°C in 900 mM caffeine solution. The transient can be fitted single exponentially with a time constant of 0.33 ns (Table IV) which is close to the one obtained for the probe in 146 mM caffeine at 25°C.

Since DCM is extremely insoluble in water and its solubility in aqueous caffeine solution is only possible due to its confinement inside caffeine dimer, the rotational time constant obtained for the probe actually signifies the time required for rotation of the caffeine in dimeric form. In view of the fact that the anisotropic time

scale is much longer compared to the obtained solvation time scales of the same sample it can be concluded that the solvation time scales obtained reflects the dynamics of the bound water around the caffeine dimer and not due to the dynamics of caffeine dimer close to one another at such a high concentration (900 mM).



Figs. 5. (a) Femtosecond resolved fluorescence transient of DCM in 900 mM caffeine at 80°C at three characteristic wavelengths. (b) Solvation correlation function,  $C(t)$  of the corresponding sample. The solid line is exponential fit. The bigger inset shows the time-resolved emission spectra (TRES) along with the anisotropy (smaller inset) of the same sample. (Reprinted with permission from ref.[36]. Copyright 2011, Springer Science + Business media)

TABLE IV  
FEMTOSECOND-RESOLVED SOLVATION CORRELATION FUNCTIONS  $C(T)$  FOR DCM AND C500 IN AQUEOUS CAFFEINE SOLUTION AT DIFFERENT TEMPERATURES(T) ALONG WITH THE CORRESPONDING ROTATIONAL RELAXATION TIME CONSTANTS ( $\tau_R$ ). ERROR  $\pm 7\%$

Aqueous caffeine solution containing probe	$T(^{\circ}\text{C})$	$C(t)$ in ps		$\tau_r$ (ps)
		$\tau_1$	$\tau_2$	
DCM	80	0.6 (82%)	5.85 (18%)	330
	20	0.8 (59%)	5.42 (41%)	55
C500	80	0.44 (94%)	25 (6%)	41

### III.1.3. Complexation of Caffeine Dimer with C500: General Picture of the Dynamics of Solvation for Caffeine Dimer

To confirm the solvation time scales around caffeine dimer at room temperature we repeated the femto second resolved experiment using another solvation probe C500 which unlike DCM is sparingly soluble in water. Since

solubility of C500 in 100 mM caffeine solution is high enough to provide good signal from the fluorophore we did not use high caffeine concentration. Molecular modeling studies (Table I and Scheme A) on the association of C500 with caffeine also reveal stacked ternary complex of two caffeine molecules and one C500 molecule. We have also checked the stability of the probe at such elevated temperature in our system and found it to be highly stable just like DCM as mentioned before. Since C500 was dissolved in 100 mM caffeine we were able to check the results both at room temperature and at 80°C. Fig. 6(a) depicts the femtosecond resolved transients at room temperature in the blue end (450 nm), peak (500 nm) and in the red end (600 nm).

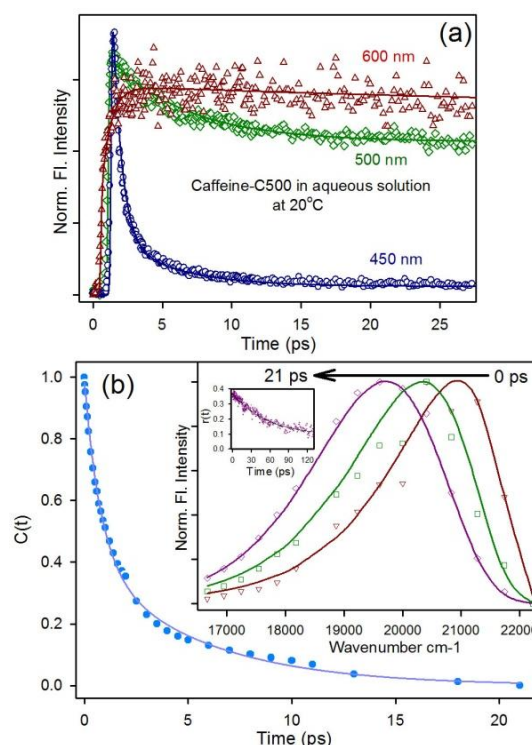
As can be observed from the Figure, the transient in the blue end can be fitted triexponentially with three decay components of 0.65 ps (82%), 4.35 ps (15%) and 5 ns (3%). On the other hand, the red end transient exhibits a distinct rise component of 0.67 ps with decay components of 57 ps and 5 ns. This is a clear indication of the solvation of the dye and we construct the TRES (see Fig. 6(b), inset) as per the procedure described in earlier section. From the time dependent Stokes shift we measure the solvent correlation function,  $C(t)$  and plot it against time (Fig. 6(b)). The curve is well fitted biexponentially with time constants of 0.8 ps (59%) and 5.42 ps (41%) (Table IV).

The recovery of similar solvation time scales even after changing the solvation probe reconfirms the dynamical nature of water molecules associated with caffeine dimer. The smaller inset inside Fig. 6(b) inset shows fluorescence anisotropy of C500 at 20°C in 100 mM caffeine solution.

The transient can be fitted single exponentially with a time constant of 55 ps (Table IV). The solvation time scales obtained at 80°C using C500 are found to be 0.44 ps (94%) and 25 ps (6%) (data not shown). The lack of significant weight of the slower component in the dynamics indicates the release of the probe C500 from the caffeine dimer to the solvent (water). Since the concerned probe C500 is sparingly soluble in water and with temperature its solubility increases, the solvation time scales thus obtained reflects the nature of dynamics of water molecules associated with the probe C500 and not with the caffeine dimer.

#### III.1.4. TNS in Caffeine Dimer: Excited State Ultrafast Charge Transfer in the Confinement

In order to investigate the consequence of the geometrical restriction of guest molecules in the caffeine dimer and the relatively slower dynamics of solvation in the interior of the dimer, we have studied excited state charge transfer reaction of a model probe TNS in the microenvironment. Upon UV excitation TNS undergoes a twisted intramolecular charge transfer (TICT) reaction, which significantly depends on the local solvation and geometrical restriction on the probe [24].



Figs. 6. (a) Femtosecond resolved fluorescence transient of C500 in 100 mM caffeine at 20°C at three characteristic wavelengths. (b) Solvation correlation function,  $C(t)$  of the corresponding sample. The solid line is exponential fit. The bigger inset shows the time-resolved emission spectra (TRES) along with the anisotropy (smaller inset) of the same sample. (Reprinted with permission from ref.[36]. Copyright 2011, Springer Science + Business media)

By observing the picosecond to nanosecond dynamics of population and polarization-analyzed anisotropy for the TNS-caffeine complex, we can also elucidate the nature of local solvation and polarity in the interior of the caffeine dimer. As shown in Table I and Scheme A, our molecular modeling reveals most stable complex of TNS with caffeine molecules to be ternary aggregate of two molecules of caffeine and one molecule of TNS in stacked geometry. It is evident that the stacking of the caffeine molecules in the close proximity of naphthalene ring offers more stabilization compared to other complex geometry.

Interaction of caffeine with TNS was studied by NMR spectroscopy. The aromatic resonances of TNS are shown in the bottommost panel of Fig. 7(a). A complete assignment of all resonances was possible using standard 2D correlation experiments. Each resonance is annotated with atom numbers consistent with Fig. 7(b). All protons showed upfield shifts upon addition of caffeine as shown in Figs. 7(a) and 7(c). The titration data were fitted with the following Eq. (19) [55]:

$$\delta_{obs} = \delta_0 + \frac{\Delta\delta^{sat}}{2K_M [T]_T} \left[ \frac{1 + K_M ([C]_T + [T]_T) + \sqrt{\{1 + K_M ([C]_T + [T]_T)\}^2 + 4K_M^2 [C]_T [T]_T}}{1 + K_M ([C]_T + [T]_T)} \right]$$

where  $\delta_{obs}$ ,  $\delta_0$  and  $\Delta\delta^{stat}$  stand respectively for TNS chemical shifts at a given caffeine concentration, in absence of caffeine and change in chemical shift in presence of large excess of caffeine;  $K_M$ ,  $[C]_T$  and  $[T]_T$  stand for caffeine-TNS association constant, total caffeine and TNS concentrations, respectively. The naphthyl ring protons (except for position 3) showed an average  $K_M$  value of  $57.4 \pm 5.7 \text{ M}^{-1}$  while the phenyl protons and H3 of the naphthyl ring showed a slightly lower  $K_M$ . These two groups of protons are also clearly different from each other when one considers the observed change in the chemical shift at 50 mM caffeine — as depicted in Fig. 7(b), the naphthyl protons showed almost double the amount of upfield shift compared to that of the phenyl group (and H3). The observed upfield shifts indicate stacking interaction between TNS and caffeine.

The greater effect felt by the naphthyl ring also indicates that caffeine mainly stacks on the naphthyl ring, which corroborates with our molecular modeling studies mentioned before. The odd behavior of the H3 proton (low net upfield shift), when compared to the behavior of all other naphthyl protons, can be explained if one considers a concomitant change in the twist of the TNS molecule upon caffeine binding.

The H3 proton, closest to the phenyl ring, experiences paramagnetic shielding / de-shielding effect of the phenyl ring, the exact nature of which will depend on the relative orientation of the naphthyl/phenyl rings. Upon caffeine binding, while all naphthyl protons feel uniform upfield shift, the H3 proton will feel an additional effect from the phenyl ring that will depend upon how the relative orientation of the naphthyl/phenyl ring (twist) changes upon complexation with caffeine. In summary, NMR experiments show the following:

- i) TNS binds caffeine with a  $K_M \sim 57 \text{ M}^{-1}$ ,
- ii) The mechanism of binding is stacking between caffeine and the TNS naphthyl ring,
- iii) Stacking is accompanied by a change of the twist angle in the TNS molecule.

Fig. 8(a) shows the steady state emission spectra of TNS ( $\lambda_{ex} = 375 \text{ nm}$ ) in water in absence and presence of caffeine. TNS is almost non-fluorescent in water (quantum yield,  $\phi_f = 0.001$ ) with a very short fluorescence life time ( $\tau_f = 60 \text{ ps}$ ) [56]. The extremely low quantum yield (0.001) in water [52],[56], indicates that the CT state dynamics are dominated by non-radiative processes, for instance, the fast intersystem crossing as proposed in the literature [57]. As evident from the Fig. 8(a) the fluorescence intensity of the probe shows a linear enhancement with increase in caffeine concentration.

The remarkable sensitivity of TNS is due to the non-radiative twisted intramolecular charge transfer (TICT) process whose rate increases very rapidly with the polarity of the medium [57]-[58].

The dramatic enhancement of the fluorescence intensity of TNS in presence of caffeine is due to the relocation of TNS molecules in the hydrophobic interior

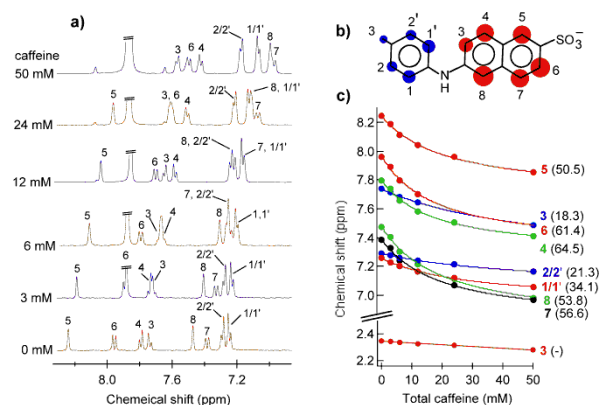
of caffeine dimers, which in turn makes the TNS molecules more rigid, retarding the TICT process in a manner comparable to cyclodextrin (CD) cavity or the micellar aggregates [59]-[61]. The binding constant ( $K_M$ ) of TNS with caffeine has been calculated from its steady state emission spectroscopy using the relation suggested by Almgren *et al.*[62]:

$$\frac{I_\infty - I_0}{I_t - I_0} = 1 + \frac{1}{K_M [M]} \quad (20)$$

where  $I_\infty$ ,  $I_t$  and  $I_0$ , denote, respectively, the emission intensities at infinite caffeine concentration, at an intermediate caffeine concentration and in the absence of caffeine,  $[M]$ , the caffeine concentration. We plot  $(I_\infty - I_0)/(I_t - I_0)$  against  $1/[M]$  which produces good linear fit (Fig. 8(b)) and  $K_M$  calculated to be  $57 \text{ M}^{-1}$  which exactly coincides with the one calculated from our NMR experiments. The binding constant of TNS with Triton X-100 (TX) micelles [56] has been reported earlier as  $3.5 \times 10^5 \text{ M}^{-1}$  while that with  $\beta$ -cyclodextrins (CD) [63]-[64] is  $2 \times 10^3 \text{ M}^{-1}$ . The observed binding constant of TNS with caffeine is orders of magnitude less compared to those with micelles and cyclodextrins, and consequently model drugs could faster be released from the caffeine dimer compared to the other hosts. The free energy change ( $\Delta G^0$ ) associated with the complex formation between TNS and caffeine using the equation can be obtained as:

$$\Delta G^0 = -RT \ln K_M \quad (21)$$

and the  $\Delta G^0$  value obtained for the present system is  $-2.4 \text{ kcal mol}^{-1}$  which is comparable to the activation energy of viscous flow (see later).



Figs. 7. (a) NMR spectra (aromatic region) of 2 mM TNS in absence and presence of caffeine (caffeine signals are capped by a double bar) at 27 C and pH 7.2. The resonances are annotated (see atom numbering shown in panel b). (b) A cartoon of TNS molecule. The relative sizes of the blue (phenyl ring) and the red (naphthyl ring) circles correspond to the relative change in chemical shift of TNS protons upon addition of 50 mM caffeine (see panel c). (c) Change in chemical shift of TNS protons upon caffeine titration. Association constants ( $K_M$ ) obtained by fitting the titration data with Eq. 19 are indicated within parenthesis (in units of  $\text{M}^{-1}$ ). (Reprinted with permission from ref.[36]. Copyright 2011, Springer Science + Business media)

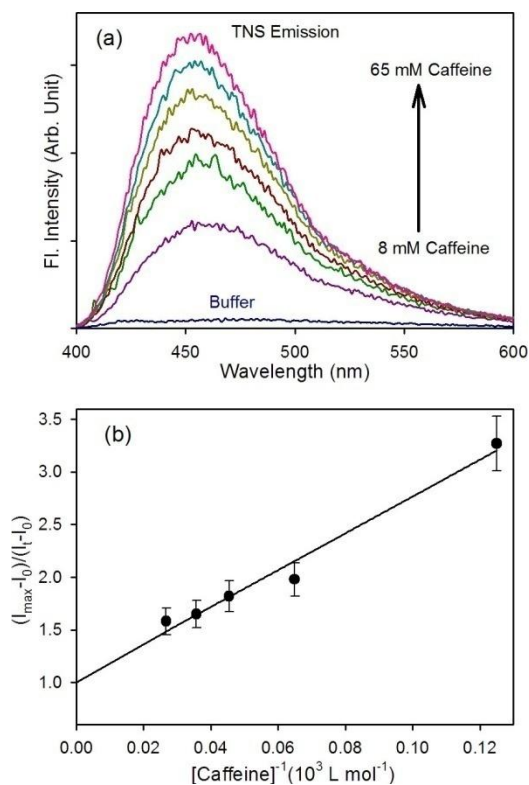


Fig. 8. (a) Emission spectra of 50  $\mu\text{M}$  TNS in absence and presence of different caffeine concentration ( $\lambda_{\text{ex}}=375\text{nm}$ ). (b) Almgren plot (see text) of TNS (50 $\mu\text{M}$ ) for various caffeine concentrations. (Reprinted with permission from ref.[36]. Copyright 2011, Springer Science + Business media)

Picosecond resolved fluorescence of TNS in presence of caffeine is presented in Fig. 9. The time resolved emission studies lend further support to the contention that TICT process of TNS gets retarded in presence of caffeine due to the confinement of the probe within the caffeine dimer because of which the lifetime of the fluorophore increases. Fig. 9 indicates that while in aqueous solution lifetime of TNS is extremely short (60 ps) [56], in presence of caffeine the fluorescence decay of TNS becomes much slower. The average lifetime of the fluorophore (Table V) increases from 60 ps in water to 168 ps and 270 ps in presence of 8 and 66 mM caffeine, respectively.

The linear enhancement in the lifetime of the fluorophore with increase in the caffeine concentration finds analogy with previous studies[59]-[61],[64] where it has been reported that the lifetime of TNS increases ~40 fold in presence of 15 mM  $\beta$ -CD compared to water.

As seen in case of CD cavity and micellar aggregates, [59],[61] the twisting motion of the probe gets restricted in presence of caffeine which results in the blockage of the nonradiative TICT process, leading to the enhancement of fluorescence lifetime.

To get more insight on the restriction of the probe in caffeine dimer, we measure the time resolved fluorescence anisotropy of TNS in water and in presence of 100 mM caffeine (Fig. 9, inset). In water the transient can be fitted single exponentially with the time constant

of 89 ps while it is 318 ps in presence of 100 mM caffeine. Applying SED (Eq. (3)) as mentioned before, the hydrodynamic volume of the probe found to be  $0.4 \times 10^{-27} \text{ m}^3$  in water and  $1.45 \times 10^{-27} \text{ m}^3$  in presence of 100 mM caffeine. The increase in the hydrodynamic volume of the probe provides evidence of the heteroassociation of the fluorophore with caffeine dimer [11] which corroborates with the molecular modeling studies represented in Scheme A and Table I and the NMR results as has been mentioned before.

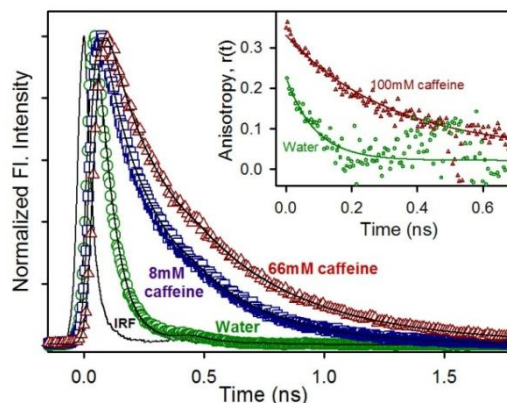


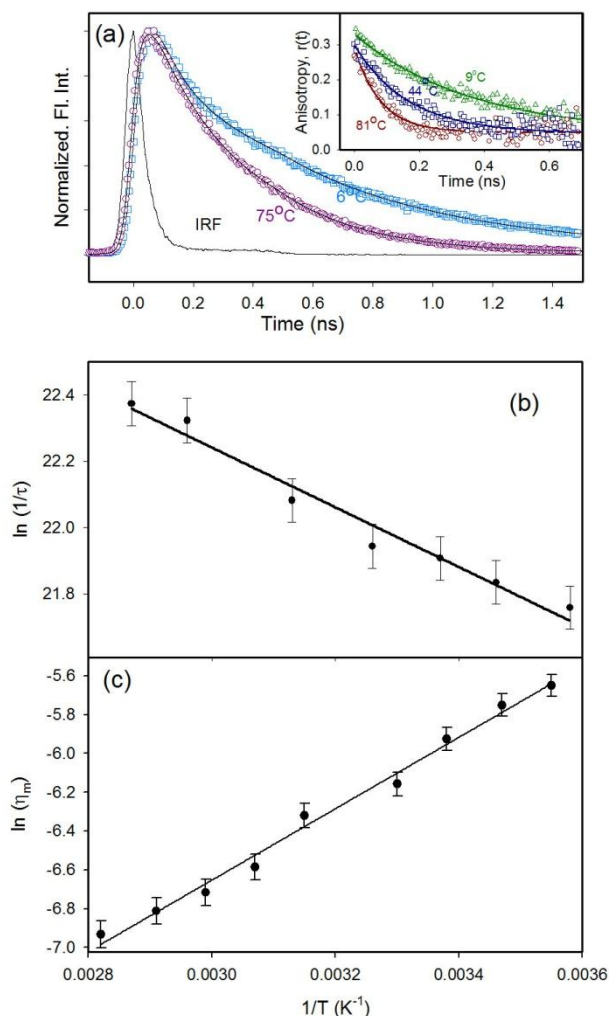
Fig. 9. Picosecond resolved fluorescence transient of TNS in water ( $\circ$ ) and in presence of 8 mM ( $\square$ ) and 66 mM ( $\Delta$ ) caffeine. The inset shows the fluorescence anisotropy of TNS in water ( $\circ$ ) and in presence of 100 mM ( $\Delta$ ) caffeine. (Reprinted with permission from ref.[36]. Copyright 2011, Springer Science + Business media)

TABLE V  
CHANGE IN FLUORESCENCE LIFETIME OF TNS WITH INCREASE IN CAFFEINE CONCENTRATION

[Caffeine] mM	$\tau_1$ (ps)	$\tau_2$ (ps)	$\tau_3$ (ps)	Average lifetime $\langle t \rangle$ (ps)
0	60 (100%)			60
8	39 (46%)	242 (48%)	567 (6%)	168
15	39 (40%)	236 (46%)	519 (14%)	197
28	39 (37%)	251 (47%)	567 (16%)	223
37	39 (35%)	237 (43%)	549 (22%)	236
46	42 (36%)	258 (45%)	594 (19%)	244
58	46 (35%)	262 (43%)	608 (22%)	263
66	50 (37%)	287 (43%)	640 (20%)	270

$\tau$  represents the time constant and the figures in the parenthesis represent relative contribution of the component. Error  $\pm 7\%$

The temperature dependent fluorescence transient of TNS in presence of 100 mM caffeine is depicted in Figures 10(a) and Table VI. The average lifetime ( $\langle \tau \rangle = \sum a_i \tau_i$  where  $\tau_i$  represents the lifetime and  $a_i$  represents the relative contribution of the  $i^{\text{th}}$  component) of the fluorophore when associated with caffeine decreases from 355 ps to 192 ps as temperature rises from 6 $^\circ\text{C}$  to 75 $^\circ\text{C}$ . Rise in temperature leading to the dissociation of TNS-caffeine complex releases TNS into the water facilitating the non-radiative TICT process which results faster fluorescence decay of the probe as observed. The result is in good agreement with the temperature dependent time resolved fluorescence anisotropy of TNS in 100 mM caffeine (Fig. 10(a), inset). The rotational time constant of TNS decreases from 363 ps at 9 $^\circ\text{C}$  to 80 ps at 81 $^\circ\text{C}$  (Table VII).



Figs. 10. (a) Temperature dependent fluorescence transients of TNS-caffeine complex at 6°C ( $\square$ ) and 75°C ( $\circ$ ). The inset shows the anisotropy of TNS in presence of caffeine at 9°C ( $\Delta$ ), 44°C ( $\square$ ) and 81°C ( $\circ$ ). (b) The plot of  $\ln(1/\tau)$  against  $1/T$  for TNS-caffeine solution. The solid line is the corresponding numerical fit of the Arrhenius equation (see text). (c) The plot of  $\ln \eta_m$  against  $1/T$  for TNS-caffeine solution. The solid line is the corresponding numerical fit of Arrhenius type plot. (Reprinted with permission from ref.[36]. Copyright 2011, Springer Science + Business media)

The ease of rotation of TNS with rise in temperature reconfirms release of TNS into water from caffeine bound state due to thermal dissociation of TNS-caffeine complex. The temperature dependence of the average lifetime of the fluorophore can be exploited to obtain the activation energy of the TICT process of the fluorophore through the Arrhenius equation [65].

Fig. 10(b) shows the Arrhenius plot for TNS in 100 mM caffeine and activation energy ( $E_{act}$ ) has been estimated as  $1.8 \pm 0.3\%$  kcal mol<sup>-1</sup>, the activation energy thus obtained reflects the energy barrier for the transition of the locally excited (LE) state to the CT state of the probe TNS. In contrast to the nearly barrierless twisting motion of the probe in pure water, the energy barrier of such motion of the probe increases upon binding to caffeine as has been observed upon binding to protein [24] due to the lower micropolarity on binding sites. In

order to estimate microviscosities we have used the simple SED (Eq. (3)). Microviscosity is the friction experienced by a probe molecule at the microscopic scale; it is an important parameter for characterizing the local environment because modest changes in local viscosity lead to variation in physical as well as chemical properties. The microviscosity changes with temperature following the relation mentioned before in Eq. (17). The plot of  $\ln \eta_m$  against  $1/T$  (Fig. 10(c)) can be linearly fitted within the experimental error of  $\pm 1\%$ . The  $E^*$  value is estimated to be 3.7 kcal mol<sup>-1</sup> which exactly corroborates with the  $E^*$  value obtained using DCM (mentioned before) in place of TNS and thus confirms that both DCM and TNS shares similar microenvironment around them in aqueous caffeine solution i.e both of them are confined within the caffeine dimer (Scheme A, Table I). It has to be noted here that the activation energy estimated for the transition of LE state to the CT state of the probe TNS is lower compared to that of the viscous flow which indicates that the CT state of the probe is stabilized by labile water molecules at higher temperature even before the probe dissociates from the caffeine dimer. The activation energy of the viscous flow along with the change in free energy associated with the complexation of TNS with caffeine gives us an idea about the amount of energy that is required to release the probe from the caffeine bound state, which is noteworthy for choosing caffeine as a tool for targeted drug delivery.

TABLE VI  
CHANGE IN FLUORESCENCE LIFETIME OF TNS IN PRESENCE OF 100 MM CAFFEINE WITH RISE IN TEMPERATURE (T)

T (°C)	$\tau_1$ (ps)	$\tau_2$ (ps)	$\tau_3$ (ps)	Average lifetime $\langle \tau \rangle$ (ps)
6	1069 (13.7%)	432 (42.2%)	60 (44.1%)	355
16	1069 (8.7%)	432 (48.6%)	60 (42.7%)	329
24	1069 (5.8%)	432 (50.5%)	60 (43.7%)	306
34	1099 (4.8%)	388 (57.1%)	54 (38.1%)	295
46	761 (7.5%)	330 (56%)	43 (36.5%)	257
65	1294 (1.6%)	299 (57.6%)	23 (40.8%)	202
75	1141 (1.7%)	259 (63.9%)	22 (34.4%)	192

$\tau$  represents the time constant and the figures in the parenthesis represent relative contribution of the component. Error  $\pm 7\%$

TABLE VII  
TEMPERATURE-DEPENDENT ROTATIONAL RELAXATION TIME CONSTANTS ( $\tau_R$ ) OF TNS IN 100 MM AQUEOUS CAFFEINE SOLUTION ( $R_0$  DEFINES ANISOTROPY AT TIME  $T = 0$ ). ERROR  $\pm 7\%$

Temperature (°C)	$r_0$	$\tau_r$ (ps)
9	0.35	363
15	0.35	321
23	0.30	262
30	0.35	203
44	0.30	165
53	0.30	123
62	0.26	105
71	0.29	93
81	0.27	80

### III.2. Ultrafast Spectroscopic Study on Caffeine Mediated Dissociation of Mutagenic Ethidium from Synthetic DNA and Various Cell Nuclei

In this section we have used steady state and picosecond resolved fluorescence spectroscopy and time gated fluorescence microscopy in order to investigate the detachment of mutagenic ethidium (Et) from synthesized DNA of specific sequences *in vitro* and various types of cell lines including squamous epithelial cells collected from the inner lining of the human mouth, A549 (lung carcinoma), A375 (human skin), RAW (macrophage) and Vero (African green monkey kidney epithelium) cells in *ex vivo* conditions.

For the investigation of the efficacy of the caffeine induced detachment of the intercalative mutagen from the DNA within and beyond the physiological temperature, we have performed temperature dependent spectroscopic measurement on the Et-DNA systems in presence and absence of caffeine molecule. A detail structural analysis employing NMR experiments followed by dynamic light scattering (DLS) studies on the caffeine-Et complex explores the molecular picture of such complexes.

Our time gated fluorescence microscopic studies on various live and fixed cell lines indicate that the efficiency of Et extraction by the xanthine alkaloid is inconsistent and not very much intuitive from the above mentioned *in-vitro* studies [22].

#### III.2.1. Detachment of Mutagenic Et from Synthesized DNA: Temperature Dependent Study

In Figs. 11(a)-(b) steady state and time resolved studies on the Et intercalated to the synthetic DNA are presented. As shown in the Fig. 11(a) Et in water produces an emission peak at 623 nm (excited at 409 nm)[66].

In presence of 100 mM caffeine, the peak exhibits a blue shift to 615 nm with a subsequent increase in the intensity. The blue shift of the emission peak signifies a hydrophobic environment experienced by Et which might be due to the caffeine-Et hetero-association as evidenced by some previous works[3],[66].

When completely intercalated in the DNA oligomer at  $[DNA]:[Et] = 8:1$ , [66] the emission of Et exhibits substantial blue shift to produce the fluorescence maximum at 600 nm with an order of magnitude increase in the intensity with respect to that in water. The observed blue shift and enhanced intensity is due to strong intercalation of Et into the hydrophobic interior of the DNA[66]. As 100 mM caffeine solution is added into the DNA-Et complex, the emission intensity decreases with a little red shift to 605 nm. The red shift can be explained in terms of the de-intercalative property of caffeine that releases certain amount of Et from the DNA bound state either to the caffeine bound state or to the free form in the buffer. Our steady state fluorescence emission results strongly corroborate with earlier studies[18].

However, conclusive spectroscopic evidences of the de-intercalated Et in the hetero-association with caffeine was absent in the earlier studies[18]. Deconvolution of the emission spectra of Et in DNA in presence and absence of caffeine suggests ~ 40% of the bound Et releases from DNA upon addition of caffeine but whether the released Et gets bound to caffeine or remains free in the solution cannot be concluded from the steady state results within such a narrow shift of emission maxima.

A similar picture evolves from the time resolved study (Fig. 11(b), Table VIII). Et in buffer shows single exponential fluorescence decay with a time constant of 1.6 ns which is close to the earlier reported values [18],[66]. In caffeine solution the decay pattern becomes biexponential with time constants of 2.3 ns (15.5%) and 7 ns (84.5%). When intercalated in DNA, the decay pattern of Et emission gets considerably slower with time constants of 1.5 ns (2%) and 21 ns (98%). Note that the insignificant contribution of the fast component in the transient confirms the presence of a very low fraction of Et free in buffer. On the other hand the longer time component (21 ns) is assigned to the lifetime of Et molecules intercalated to DNA[66]. When 100 mM caffeine is added to Et-DNA complex the decay process becomes faster and can only be fitted triexponentially with time constants of 1.8 ns (4%), 7 ns (22%) and 23 ns (74%). These time constants can easily be identified with those of Et in buffer, hetero-association with caffeine and intercalation with DNA, respectively and fits to the heterogeneous model of Et in the aqueous solution of DNA in presence of caffeine. The triexponential nature of the decay pattern signifies the presence of at least three different environment of residence of Et in the solution. If the contribution from each environment is assumed to add up linearly in the total decay process, then it can be inferred that addition of caffeine reduces the fraction of Et molecules bound to DNA from 98% to 74% and the released Et mostly gets bound to caffeine as indicated by the 7 ns component (22%) and a small fraction (2%) goes into the buffer.

The uncertainty range in the lifetime measurements is  $\pm 7\%$ . Our experimental result strongly upholds the de-intercalative activity of caffeine reported by Johnson et al.[18] However, our work finds inimitability in characterising the 7ns component (characteristic lifetime of Et complexed with caffeine) which further clarifies the process. By measuring the relative weightage of the 21 ns component, which is a signature of the total population of Et bound to DNA, and knowing the total concentration of Et and DNA molecules in the solution, we calculate the binding constant ( $K$ ) of the ligand Et with DNA using the following equation [66]:

$$K = \frac{[Et - DNA]}{([Et] - [Et - DNA]) \times ([DNA] - [Et - DNA])} \quad (22)$$

where  $[Et - DNA]$ ,  $([Et] - [Et - DNA])$ ,  $([DNA] - [Et - DNA])$  represents concentration of Et-DNA complex, free Et and

free DNA in the solution respectively.

The binding constant of Et with DNA is calculated to be  $15.4 \pm 1.1 \times 10^4 \text{ M}^{-1}$  which is comparable to the binding constant value of Et with genomic DNAs reported earlier [66]-[67]. In presence of caffeine the binding constant value reduces to  $7.6 \pm 0.5 \times 10^3 \text{ M}^{-1}$  as part of the free Et is sequestered by free caffeine leading in this way to a shift of the equilibrium between Et not bound to DNA and Et bound to DNA, whereas the value for caffeine solution is calculated to be  $54.6 \pm 3.8 \text{ M}^{-1}$  which is also in close approximation of that reported earlier[67]. We calculate the free energy change associated with the complex formation using the equation:

$$\Delta G^0 = -RT \ln K \quad (23)$$

and it is found that the difference in the free energy between the intercalated Et ( $-29.6 \pm 0.2 \text{ KJ mol}^{-1}$ ) and Et-DNA-caffeine complex ( $-22.15 \pm 0.15 \text{ KJ mol}^{-1}$ ) is more than compensated by the binding of Et with caffeine ( $-9.9 \pm 0.2 \text{ KJ mol}^{-1}$ ), which makes the de-intercalation process of caffeine energetically favourable.

TABLE VIII  
THE LIFETIME COMPONENTS ( $\tau_1, \tau_2, \tau_3$ ) WITH CORRESPONDING AMPLITUDES ( $A_1, A_2, A_3$ ) OF ET IN VARIOUS ENVIRONMENTS; ERROR  $\pm 5\%$

Sample	$\tau_1$ (ns)	$A_1\%$	$\tau_2$ (ns)	$A_2\%$	$\tau_3$ (ns)	$A_3\%$
Et in buffer	1.6	100				
Et in 100 mM caffeine	7	84.5	2.3	15.5		
[Et]:[DNA] = 1:8	1.5	2	21	98		
[Et]:[DNA] = 1:8 in presence of 100 mM caffeine	7	22	23	74	1.8	4

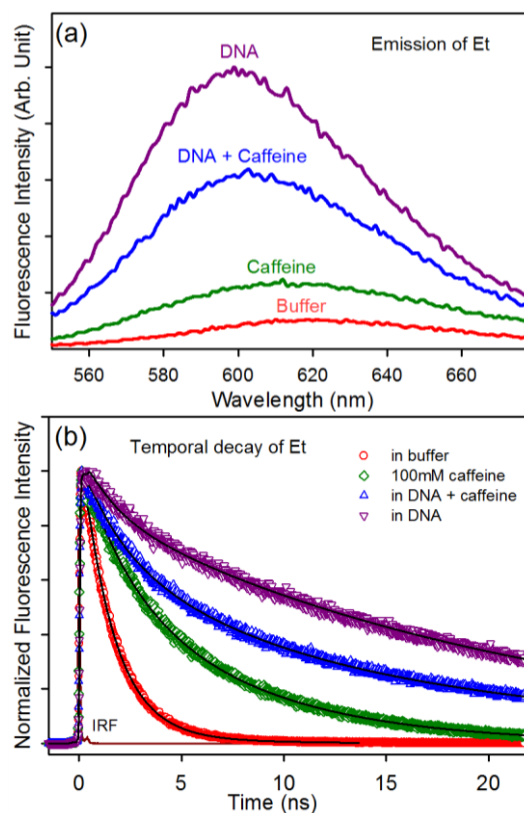
To determine the thermal stability of the caffeine-Et complex we perform temperature dependent time resolved experiments (Figs. 12). We first monitor the release of DNA intercalated Et into the buffer with rise in temperature as depicted in Fig. 12(a). As the temperature rises DNA melts with subsequent release of the intercalated Et into buffer as evidenced through the rise in amplitude of the faster lifetime component of  $\sim 2 \text{ ns}$  from 3% to 45% as temperature rises from 18 to  $71^\circ\text{C}$  (Table IX).

Upon addition of 100 mM caffeine in the DNA – Et system we monitor the temperature dependent change in the lifetime of the Et as shown in Fig. 12(b) and Table X.

While in the absence of caffeine, Et is released from the intercalated to the free state in buffer with the progress in DNA melting, in presence of caffeine most of the released Et, from the DNA intercalated state, heteroassociates with the available caffeine in the solution as has been observed from the rise in the amplitude of the lifetime component of Et characteristic of its hetero-association with caffeine, with minor rise in the amplitude of the faster component of  $\sim 2 \text{ ns}$  from 5% to 14% over the same range of temperature.

Since most of the released Et from the DNA bound state remains in a strong hetero-association with the

caffeine molecules in the solution even at high temperature at around  $71^\circ\text{C}$  it can be concluded that the complex that forms between caffeine and Et is thermally stable and caffeine can perform its de-intercalative activity even at high temperature.



Figs. 11. (a) Steady state emission of ethidium in various environments. (b) Time resolved fluorescence transients of ethidium (from bottom) in buffer, caffeine ([caffeine] = 100 mM), DNA ([DNA]:[Et] = 8:1) in presence and absence of caffeine. (Reprinted with permission from ref.[22]. Copyright 2011, American Chemical Society)

For further confirmation of the thermal stability of the caffeine-Et complex we monitor the temperature dependent fluorescence transient of Et in presence of high caffeine concentration (Fig. 12(b) inset and Table XI). As depicted in Fig. 12(b) (inset) and Table XI the amplitude of the faster component of  $\sim 2 \text{ ns}$ , which represents the fraction of free Et present in buffer, does not change with rise in temperature which reconfirms the high stability of caffeine-Et complex both within and beyond the physiological temperatures.

TABLE IX  
VARIATION OF FLUORESCENCE TRANSIENTS OF DNA BOUND ET ([DNA]:[Et] = 8:1) WITH TEMPERATURE:  $\tau$  REPRESENTS THE TIME CONSTANT AND A REPRESENTS RELATIVE CONTRIBUTION OF THE COMPONENT. ERROR  $\pm 5\%$

Temperature ( $^\circ\text{C}$ )	$\tau_1$ (ns)	$A_1\%$	$\tau_2$ (ns)	$A_2\%$
18	22	97	2.1	3
30	22	95	2.1	5
42	21	95	1.6	5
52	20	91	1.5	9
61	19	79	1.4	21
71	18	55	1.4	45

TABLE X  
VARIATION OF FLUORESCENCE TRANSIENTS OF DNA BOUND ET ([DNA]:[ET] = 8:1) WITH TEMPERATURE IN PRESENCE OF 100 MM CAFFEINE;  $\tau$  REPRESENTS THE TIME CONSTANT AND A REPRESENTS RELATIVE CONTRIBUTION OF THE COMPONENT. ERROR  $\pm 5\%$

Temperature (°C)	$\tau_1$ (ns)	A <sub>1</sub> %	$\tau_2$ (ns)	A <sub>2</sub> %	$\tau_3$ (ns)	A <sub>3</sub> %
18	22	60	7	35	1.7	5
30	22	57	6.4	38	1.5	5
42	22	46	6.05	48	1.35	6
52	22	35	5.67	58	1.36	7
61	22	21	5.5	65	1.69	14
71	22	10	4.68	76	1.5	14

TABLE XI  
VARIATION OF FLUORESCENCE TRANSIENTS OF ET (12.5  $\mu$ M) WITH TEMPERATURE IN PRESENCE OF 100 MM CAFFEINE;  $\tau$  REPRESENTS THE TIME CONSTANT AND A REPRESENTS RELATIVE CONTRIBUTION OF THE COMPONENT. ERROR  $\pm 5\%$

Temperature (°C)	$\tau_1$ (ns)	A <sub>1</sub> %	$\tau_2$ (ns)	A <sub>2</sub> %
18	7.15	88	2	12
30	6.6	89	1.8	11
41	6.06	89	1.7	11
50	5.56	88	1.7	12
61	5	88	1.6	12
71	4.4	88	1.5	12

### III.2.2. Exploration of the Molecular Picture of Caffeine-Et Complex

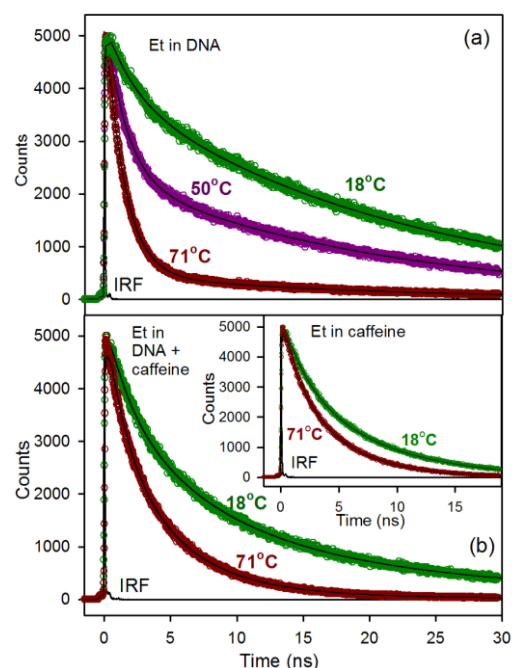
The mode of interaction of caffeine with the DNA intercalator Et was studied using NMR spectroscopy. All observable protons in Et and caffeine were assigned and were followed in a NMR experiment where 1.78 mM Et was titrated with caffeine. The changes in the chemical shift of Et protons ( $\Delta\delta_{obs} = \delta_{with\ caffeine} - \delta_{no\ caffeine}$ ) are shown in Fig. 13(a).

All proton signals (the Et CH<sub>2</sub> signal overlapped with H<sub>2</sub>O signal and was not monitored) exhibited a hyperbolic change indicating Et-caffeine binding. Changes in  $\Delta\delta_{obs}$  of individual<sup>1</sup> H-chemical resonances in Et, upon titration with caffeine, were fitted with Eq. (24)[55] (which is a modified form of the Eq. (19)) for obtaining the association constant  $K_a$  ( $[C]_T$  and  $[E]_T$  are the total concentrations of caffeine and Et respectively and  $\Delta\delta^{max}$  is the value of  $\Delta\delta_{obs}$  for a large excess of  $[C]_T$ ):

$$\Delta\delta_{obs} = \frac{\Delta\delta^{max}}{2K_a[E]_T} \left[ \frac{1 + K_a([C]_T + [E]_T) + \sqrt{\{1 + K_a([C]_T + [E]_T)\}^2 + 4K_a^2[C]_T[E]_T}}{2} \right] \quad (24)$$

As can be observed from Figure 13(a),  $K_a$  values were different depending on which protons one monitored;  $K_a \sim 12\text{ M}^{-1}$  (positions 4 and 7),  $\sim 20\text{ M}^{-1}$  (positions 2 and 9),  $\sim 30\text{ M}^{-1}$  (positions 1 and 2) and  $\sim 65\text{-}73\text{ M}^{-1}$  (for CH<sub>3</sub> and the ortho proton of Et benzene ring); the latter matching best with the estimate from time-resolved data (this work) and a previous report based on UV-Vis absorption spectroscopy. The range of  $K_a$  values obtained from NMR spectroscopy reflects structural heterogeneity

of the Et:caffeine complex, undetected by optical spectroscopy. This is consistent with the broad distribution observed from DLS studies around a dominant conformation (discussed later; see Fig. 15(a)).

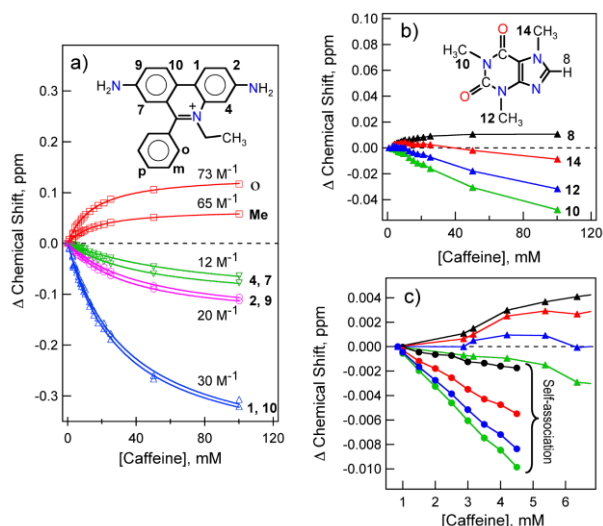


Figs. 12. Temperature dependent time resolved fluorescence transients of (a) [DNA]:[Et] = 8:1 in absence and (b) in presence of caffeine ([caffeine] = 100 mM) and 12.5  $\mu$ M Et in presence of caffeine (inset (b)). (Reprinted with permission from ref.[22]. Copyright 2011, American Chemical Society)

The nature of the dominant conformation can be understood by a careful analysis of ring current shifts observed in Et as a function of added caffeine. During Et-caffeine interaction, the degree of change in  $\Delta\delta_{obs}$  (and  $K_a$ ) varied in a symmetric fashion (equivalence of 1-10, 2-9 and 4-7 positions) across Et molecule. In addition, while positions 1, 10, 2, 9, 4 and 7 exhibited a negative  $\Delta\delta_{obs}$ , the benzyl ortho position and the CH<sub>3</sub> protons of Et showed a positive  $\Delta\delta_{obs}$ . The major cause of chemical shift change in Et, due to interaction with caffeine, must originate from ring current shifts, producing positive and negative  $\Delta\delta_{obs}$ .

Placement of an Et proton directly above the caffeine ring (stacking) will produce a negative  $\Delta\delta_{obs}$  while positioning of Et protons in the plane of the caffeine ring will produce a positive  $\Delta\delta_{obs}$ . Based on the NMR data (symmetry of  $K_a$  and  $|\Delta\delta_{obs}|$ ) and the assumption that the sign of  $\Delta\delta_{obs}$  originates from the ring current effect, a model for a 1:1 complex of caffeine:Et was constructed as shown in Fig. 14(b).

Caffeine and Et molecules are stacked in the 1:1 model where the CH<sub>3</sub> and the ortho-benzyl protons of Et (shown as magenta spheres in Fig. 14(b)) protrude towards the plane of the caffeine ring giving rise to the observed positive  $\Delta\delta_{obs}$ . The stacked caffeine can flip, effectively making its effect on the Et symmetric.



Figs. 13.  $^1\text{H}$ -chemical shift changes observed during titration of Et (1.78 mM) by caffeine (pH 7.0, 25°C): a) Et, b) caffeine.  $^1\text{H}$  resonance signals are annotated with atom numbers, corresponding to the molecules shown in the panels. The continuous lines in panel (a) correspond to the best fits with Eq. 24 with the corresponding  $K_a$  values reported above each fit. Panel (c) shows changes in caffeine  $^1\text{H}$ -chemical shifts for early data points (0-6 M) of panel (b) along with  $^1\text{H}$ -chemical shift changes in caffeine due to self-association (concentration dependence) in the same concentration range. Atom numbering (colors) in panel (c) is identical to that in panel (b). (Reprinted with permission from ref.[22]. Copyright 2011, American Chemical Society)

The flipping is consistent with a model of caffeine dimer where two forms of caffeine dimers (flipped and un-flipped stacking, Fig. 14(a)) have been observed[68]. Our model suggests that two protons in caffeine, positions 8 and 14 (shown as magenta spheres in Fig. 14(b)), should also exhibit a positive  $\Delta\delta_{obs}$  (ring current effect from Et).

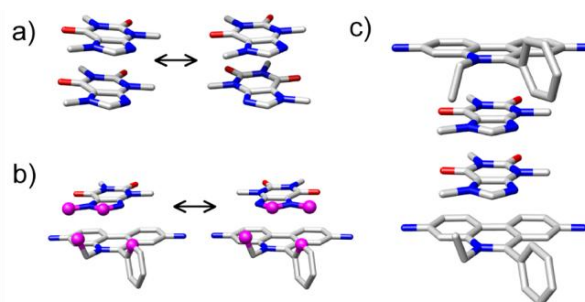
To validate this, caffeine chemical shifts were monitored in the Et titration experiment of Fig. 13(a) and are shown in Fig. 13(b). Indeed positions 8 and 14 of caffeine showed a positive  $\Delta\delta_{obs}$  as expected from the model. This becomes more clear in Fig. 13(c) where the early data points are shown (up to 4:1 caffeine:Et ratio) along with caffeine self association data (all resonance in the self association show negative  $\Delta\delta_{obs}$ ).

In order to determine the size of the complex formed between caffeine and Et, we performed DLS experiments and the results are shown in Fig. 15(a).

The DLS data, with broad peaks for caffeine, in presence and in absence of Et, indicate a distribution of populations around a dominant structure and consistent with NMR data. The DLS-derived hydrodynamic diameter (corresponding to the peak of the distributions) of 100 mM caffeine is 8.4 Å.

This increases to 14.2 Å upon addition of 25 μM Et. Fluorescence anisotropic studies on Et (Fig. 15(b)), in presence of caffeine, yielded a hydrodynamic diameter of 12.3 Å, slightly lower than the DLS-derived value.

To compare with the experimental values, hydrodynamic diameters of caffeine dimer (Figure 14(a)) and the 2:2 caffeine-Et complex (Figure 14(c)) were estimated using the program Hydropro [69].



Figs. 14. a) Inter-converting caffeine dimers (stacked on each other). b) A model for inter-converting 1:1 complex of caffeine and Et, compatible with NMR titration data.  $^1\text{H}$ -resonances that exhibited upfield shift upon complex formation (positions 8 and 14 in caffeine, and o and Me in Et; Figure 13) are shown as ball and stick model (magenta). c) A model of 2:2 caffeine:Et complex compatible with caffeine:caffeine stacking (panel a) and caffeine:Et stacking (panel b). The structures were energy minimized to remove steric clashes. (Reprinted with permission from ref.[22]. Copyright 2011, American Chemical Society)

The calculated diameters, 8.9 Å for caffeine dimer, and, 13.0 Å for the 2:2 caffeine-Et complex, are compatible with the experimental data.

The above analysis shows that the major component of pure caffeine is the dimeric form. In presence of Et, caffeine:Et complexes with a 2:2 (or higher) stoichiometry dominates. Incidentally, no peaks were obtained at higher hydrodynamic radii indicating the absence of any higher order aggregation.

### III.2.3. Efficiency of Caffeine in the Expulsion of Et from Various Cell Lines: Time Gated Fluorescence Microscopic Studies

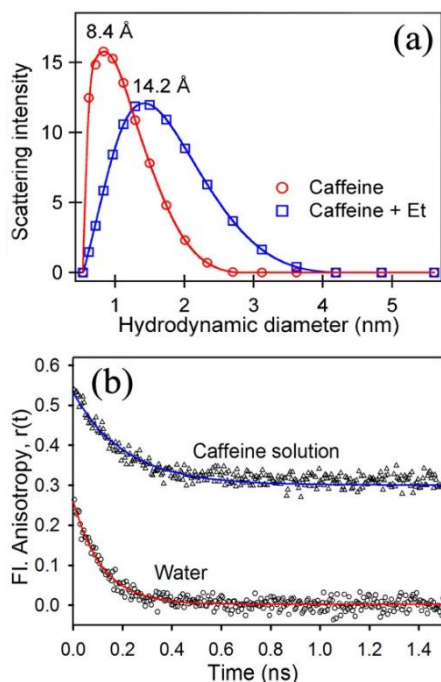
Our spectroscopic results reflecting the efficacy of caffeine in the extraction of Et upon forming a caffeine-Et complex with it provoke us to get a microscopic view of such activity of caffeine molecules.

In order to study in biological milieu we have used some animal cell lines. Fig. 16(a) shows the fluorescence micrographs of both live and fixed A549 cells stained with Et and subsequently treated with caffeine (+ caffeine) and for control experiment identical sets of stained cells were treated with PBS without caffeine (- caffeine).

Comparing the fluorescence micrographs of both live and fixed '+ caffeine' and '- caffeine' cells after 60 seconds of treatment we observe there is a significant drop in the emission intensity of Et from the nucleus of the live A549 cells treated with caffeine.

The drop in emission intensity of Et can be explained in terms of the efficiency of caffeine molecules in removal of Et from the nucleus of those live cells. As evident from the fluorescence micrographs of Figure 16(a), the efficacy of caffeine in the extraction of Et from the nucleus of fixed cells is less compared to the live ones. In order to get an insight on the kinetics of the extraction process we plot  $I_{(t)}/I_{(0)}$  against time (Figure 16(b)), where  $I_{(t)}$  represents emission intensity of Et in nucleus at time t and  $I_{(0)}$  represents the same initially just

after the addition of caffeine to the live A549 stained cells. We fit the curve with single exponential decay and find the extraction of Et from the cell nucleus of live A549 cells by caffeine with a characteristic time constant of 38 seconds.



Figs. 15. (a) Dynamic light scattering of 100 mM caffeine with (blue squares) and without (red circles) 25  $\mu$ M ethidium. (b) Fluorescence anisotropy of Et in water ( $\circ$ ) and in presence of 100 mM ( $\Delta$ ) caffeine. The base line for anisotropy of Et in caffeine solution has been shifted vertically by 0.3 for better clarity. (Reprinted with permission from ref.[22]. Copyright 2011, American Chemical Society)

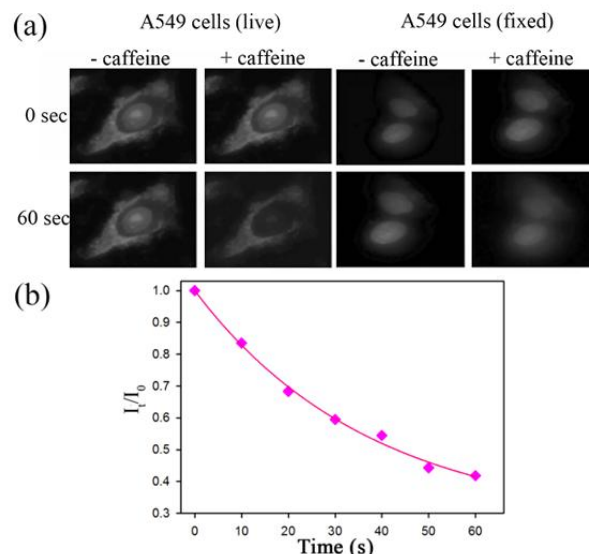
After monitoring the effect of caffeine on A549 cells we proceed with squamous epithelial cells taken from human mouth. Et being a potential intercalator of DNA[70], binds only in the nucleus of the cell and the red emission observed in the micrographs (Figure 17b upper right inset) are due to the Et that emits in the red region ( $\sim 600$ nm)[66].

As can be observed from the Figure, when the stained cells are treated with caffeine (+ caffeine), Et is released from the nucleus at a very fast rate.

The intensity of red colour of the cells is blurred with time which indicates release of Et from the nucleus. In control experiment (- caffeine) cells retain almost the entire amount of Et in their nucleus. In order to highlight the de-intercalative property of caffeine in a more quantitative manner, the intensity of the red colour of Et from cell nucleus, which is proportional to the amount of Et present, has been plotted at regular time interval for both the systems ('- caffeine' and '+ caffeine') where the x-coordinate represents distance in the horizontal plane where the cell lies (Fig. 17(a)).

As evident from the Figure the intensity of red colour is considerably high at the position that corresponds to the cell nucleus and it falls rapidly after 8 seconds (blue line) upon treatment with caffeine solution, whereas a

negligible change is produced in control set (- caffeine) within the same time scale (Fig. 17(a), inset).



Figs. 16. (a) Fluorescence micrographs of both live and fixed Et stained A549 cells initially and after 60 seconds upon treatment with caffeine (+ caffeine) along with the control sets (- caffeine) treated with PBS without caffeine. (b) Rate of leaching out of Et from nucleus of live A549 lung carcinoma cells when treated with caffeine.  $I_t$  and  $I_0$  represents the emission intensity of Et at time  $t$  and initially, respectively. (Reprinted with permission from ref.[22]. Copyright 2011, American Chemical Society)

After 18 seconds, '+ caffeine' cells show negligible amount of Et left in their nucleus (green line) while no significant change has been observed in '- caffeine' cells.

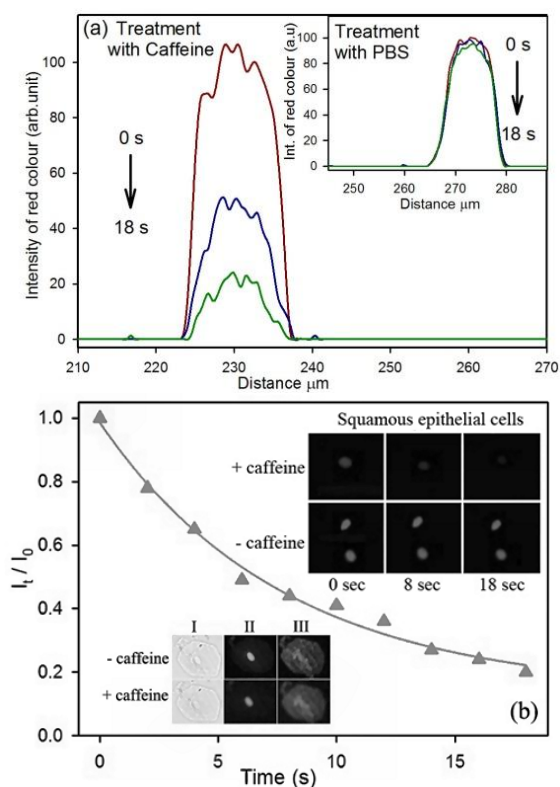
As a control study to rule out the possibility of cell disruption upon treatment with caffeine, we have taken the cell images (Fig. 17(b), lower left inset) under bright field before and after treating them with caffeine and found no change even after 5 minutes. In addition, we stained the cell nuclei with a fluorescent dye, DAPI and found that cell nuclei remain intact over the same time span upon treatment with caffeine.

Furthermore, we checked the membrane integrity of the cells by staining them with another fluorescent dye, merocyanine 540 and found that the cell membranes remain unperturbed upon treatment with caffeine. The plot of  $I_t/I_0$  against time (Fig. 17(b)), gives the characteristic time constant for extraction of Et from these cells by caffeine as 8 seconds.

However no significant result has been observed in the removal of Et from A375, RAW and Vero by caffeine (Fig. 18).

### III.3. Caffeine Mediated Detachment of Mutagenic Ethidium from Various Nanoscopic Micelles: An Ultrafast FRET Study

In the present section we have used ethidium (Et) bromide salt as model ligand probe, which is a well known DNA intercalator [35],[66] and a potential mutagen[17].



Figs. 17. (a) Reduction in intensity of red colour with time when squamous epithelial cells treated with caffeine and PBS as control (inset). (b) Rate of leaching out of Et from nucleus of squamous epithelial cells when treated with caffeine.  $I_t$  and  $I_0$  represents the emission intensity of Et at time  $t$  and initially, respectively. Upper right inset shows the fluorescence micrographs of Et stained same cells initially, after 8 seconds and after 18 seconds upon treatment with caffeine along with the control sets. Lower left inset shows the morphology of the same cell line before and after 5 minutes upon caffeine treatment under bright field (I) and fluorescence micrographs of the same stained with DAPI (II) and Merocyanine 540 (III). (Reprinted with permission from ref.[22]. Copyright 2011, American Chemical Society)

The micelles used in our study are cationic hexadecyltrimethylammonium bromide (CTAB), neutral (polar) Triton X-100 (TX-100) and anionic sodium dodecyl sulphate (SDS) with distinct hydrodynamic diameter as measured by dynamic light scattering (DLS) experiment. The probe Et shows distinct spectroscopic signature, particularly excited state lifetime in various biologically relevant environments. We have used steady state and picosecond resolved fluorescence spectroscopy in order to investigate the detachment of Et from various self-organized micelles.

In the case of DNA mimicking SDS micelles we have used another probe Hoechst 33258 (H258) as energy donor to Et acceptor at the surface and employ Förster resonance energy transfer (FRET) for the analysis of fluorescence quenching of the donor H258.

Standard FRET analysis on the donor-acceptor (D-A) pair at the SDS micelles shows significant perturbation on the energy transfer efficiency upon addition of caffeine in the solution. Further analysis of the experimental results employing both the general and extended version of well known 'Infelta-Tachiya model'

distinctly reveals change in acceptor distribution at the micellar surface in the presence of caffeine in the aqueous solution. We have used DLS in order to confirm the structural integrity of the micelles in the caffeine solution. Furthermore, we have employed fluorescence microscopy to monitor the said perturbation in FRET efficiency on squamous epithelial cell nuclei in presence of caffeine [71].

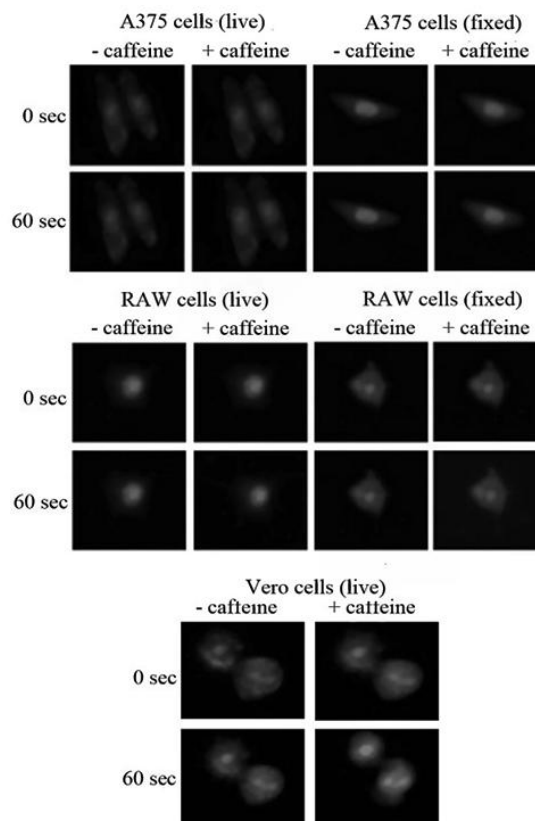


Fig. 18. Fluorescence micrographs of Et stained A375 and RAW cells (both live and fixed) along with Vero (live) cells treated with caffeine (+ caffeine) and images taken at 0 second and 60 seconds interval. The control sets (- caffeine) treated with PBS without caffeine. (Reprinted with permission from ref.[22]. Copyright 2011, American Chemical Society)

### III.3.1. Caffeine Mediated Detachment of Et from Various Self-Organized Micelles

Fig. 19(a) shows the fluorescence transients of the mutagenic ethidium (Et) in various micellar systems of different charge nature in absence and presence of caffeine. Both Et and CTAB being cationic, ionic interaction between the two will not be favoured but the possibility of hydrophobic interaction between them cannot be ruled out. This was the reason behind our selection of cationic CTAB and neutral (polar) TX-100 micelles. As evidenced from our lifetime results (given Table XII), beyond the critical micelle concentration (CMC) of CTAB, Et interacts with the micelles to some extent which is only possible through its interior binding. Et in the cationic CTAB micelles reveals fluorescence

lifetimes of 1.4 ns (51%) and 2.5 ns (49%). However, on addition of caffeine in the solution, the lifetime values become 1.9 ns (14%) and 7.2 ns (86%) revealing a major slower component (7.2 ns), characteristic of Et-caffeine complexation (Table XIII).

The faster component is close to the lifetime of Et in water which is  $\sim 1.5$  ns[66]. In the case of anionic SDS micelles significant detachment of Et in the caffeine solution is also evident (Fig. 19(a) and Table XIII).

Our SDS concentration dependent absorption studies along with the time resolved fluorescence and anisotropy measurements on Et both in absence and presence of caffeine (Fig. 20 and Table XIV) is in good agreement with the model where Et attaches to SDS micelles with its positively charged moiety towards the negatively charged head group of the SDS micelles and hydrophobic part inside the micelles. From the difference in optical density (O.D) value of Et in SDS micelles in absence and presence of caffeine we calculated the amount of Et released from the micelles by caffeine taking the molar extinction coefficient of Et in SDS micelles as  $4120 \text{ M}^{-1} \text{ cm}^{-1}$  at 476 nm. It has been found that from  $25 \mu\text{M}$  micelle-bound EtBr,  $18.5 \mu\text{M}$  of Et gets released from the micelles by caffeine while  $6.5 \mu\text{M}$  Et still remains attached to the micelles.

As evidenced from the UV-vis absorption spectra along with the fluorescence lifetime and anisotropy measurements of Et at different concentrations of neutral (polar) surfactant TX-100 (Figure 21 and Table XV), Et neither binds to TX-100 monomers nor to TX-100 micelles at lower concentrations ( $8.2 \times 10^{-3}$  mM micellar concentration).

However, at high micellar concentration (1mM), we observe bathochromic shift in the absorption peak of Et compared to that in water which reflects association of Et with TX-100 micelles positioning the quaternary Nitrogen of Et towards the hydrophilic head group of the micelles i.e towards the ethylene oxide part (Fig. 22) and hydrophobic part being buried inside. The proposed model corroborates with the fluorescence anisotropy results (Table XV) where we find longer rotational time constant of Et at 100 mM TX-100 concentration.

However, detail analysis of the absorption and time resolved spectroscopy results show that caffeine fails to detach Et from TX 100 micelles unlike SDS and CTAB micelles. Our DLS studies on differently charged micellar systems (Fig. 19(b)) show the structural integrity of the micelles both in absence and presence of caffeine. Since the hydrodynamic radii of the micelles remain similar even after the addition of caffeine, it can be concluded that caffeine molecules are not associated with the micelles.

In order to show the detachment of Et at the molecular level from the anionic SDS micelles, which is considered to be mimic of the DNA surface [26], we have employed Förster resonance energy transfer (FRET) from another ligand H258 on the surface of the micelles to the bound Et. The FRET which is known to be molecular ruler[72] is an effective technique to find out the distance between

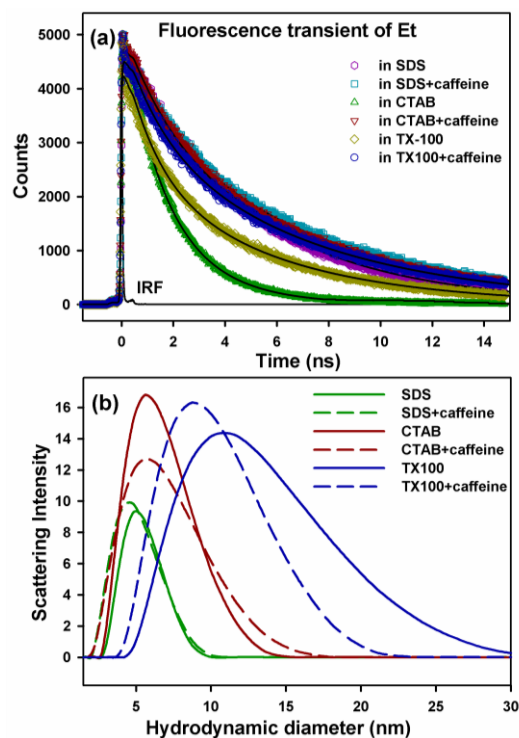
two ligands, donor and acceptor, having overlap of the emission and absorption spectrum of the donor and acceptor respectively.

Figs. 23 show that there is sufficient spectral overlap between the emission spectrum of the H258 and the absorption spectrum of the Et in SDS micelles both in absence and presence of caffeine.

As shown in the Figure,  $J(\lambda)$ , the overlap integral, which expresses the degree of spectral overlap between the donor emission and the acceptor absorption changes in presence of caffeine. The minor groove binder H258 shows single exponential fluorescence decay of 3.38 ns in SDS micelles (Fig. 24(a), Table XVI).

Previous work from our group[27] finds the location of H258 on the surface of SDS micelles and not in the interior of it based on steady state emission and time resolved anisotropy studies of the probe in the micellar environment. Presence of Et (acceptor) in the solution makes the decay faster (867 ps (17%) and 98 ps (2%)) (Table XVI), revealing simultaneous binding of H258 and Et in the micellar surface with average distance of 2.16 nm, consistent with earlier studies [35].

The fast time component  $\tau_3$  listed in Table XVI is around IRF however, within the resolution of our TCSPC setup. The binding of Et on the surface of SDS micelles is also reasonable from the time resolved studies reported earlier [73] where the fluorescence lifetime and relative quantum yield of Et, bound to SDS, are shown to be intermediate between those in water and in alcohol reflecting that Et binds to the surface of anionic SDS micelles due to its inherent positive charge.



Figs. 19. (a) Fluorescence transient of Et in SDS, CTAB and TX-100 micellar systems and (b) diameter size of those micelles, in presence and absence of caffeine. (Reprinted with permission from ref.[71]. Copyright 2012, American Chemical Society)

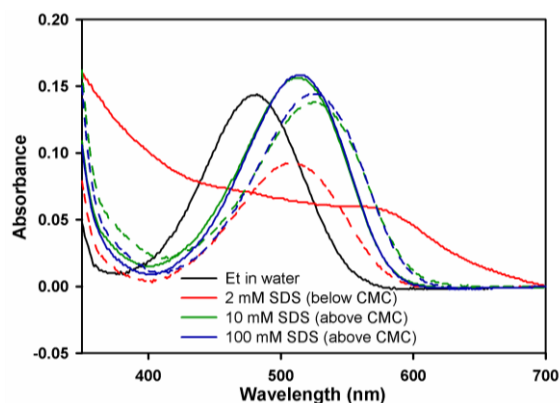


Fig. 20. Absorption of ethidium (Et) at different concentrations of SDS with (broken line) and without (bold line) caffeine. (Reprinted with permission from ref.[71]. Copyright 2012, American Chemical Society)

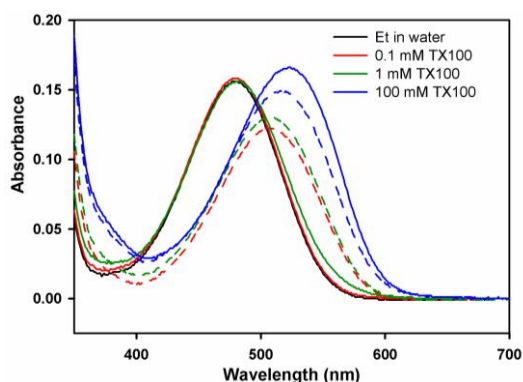


Fig. 21. Absorption of ethidium (Et) at different concentrations of TX-100 with (broken line) and without (bold line) caffeine. (Reprinted with permission from ref.[71]. Copyright 2012, American Chemical Society)

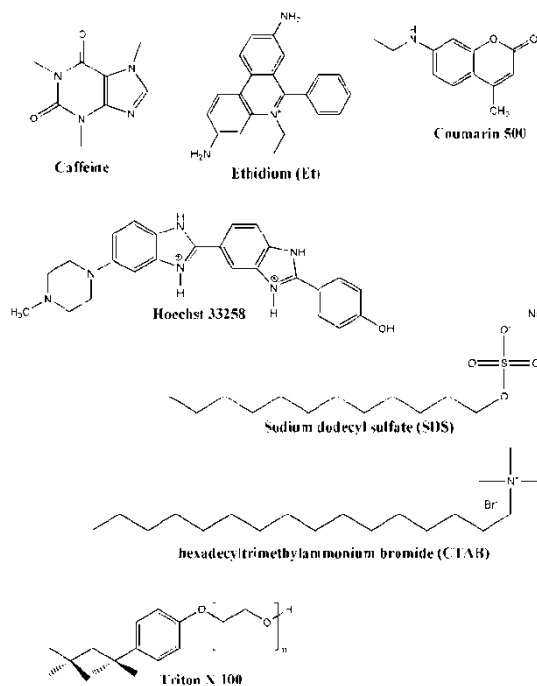


Fig. 22. Structures of the caffeine, dyes Hoechst 33258 (H258), Coumarin 500 (C500), ethidium (Et) and surfactants SDS, CTAB and Triton X 100 (TX-100). (Reprinted with permission from ref.[71]. Copyright 2012, American Chemical Society)

TABLE XII  
THE FLUORESCENCE LIFETIME COMPONENTS  $\tau_1$  AND  $\tau_2$  REPRESENT FLUORESCENCE LIFETIMES OF THE SAMPLE WHILE  $\tau_R$  REPRESENTS ROTATIONAL RELAXATION TIME CONSTANTS OF THE SAME AND  $R_0$  DEFINES ANISOTROPY AT TIME  $T=0$ . FIGURES IN PARENTHESES SHOW RELATIVE CONTRIBUTION. ERROR  $\pm 5\%$

Et in	$\tau_1$ (ns)	$\tau_2$ (ns)	Fluorescence anisotropy	
			$\tau_r$ (ns)	$I_0$
water	1.6 (100%)		0.110	0.24
100 mM caffeine	2.3 (15%)	7.0 (85%)	0.210	0.23
0.2 mM CTAB	1.6 (100%)		0.100	0.30
0.2 mM CTAB + 100 mM caffeine	1.7 (13%)	6.9 (87%)	0.170	0.34
0.4 mM CTAB	1.6 (100%)		0.110	0.35
0.4 mM CTAB + 100 mM caffeine	1.7 (14%)	7.0 (86%)	0.180	0.34
0.6 mM CTAB	1.6 (100%)		0.110	0.32
0.6 mM CTAB + 100 mM caffeine	1.8 (15%)	6.9 (85%)	0.160	0.37
2 mM CTAB	1.1 (34%)	1.9 (66%)	0.100	0.32
2 mM CTAB + 100 mM caffeine	1.8 (14%)	6.9 (86%)	0.170	0.38
20 mM CTAB	1.2 (45%)	2.1 (55%)	0.110	0.32
20 mM CTAB + 100 mM caffeine	1.8 (14%)	6.9 (86%)	0.180	0.35
40 mM CTAB	1.2 (40%)	2.0 (60%)	0.120	0.29
40 mM CTAB + 100 mM caffeine	1.7 (14%)	6.9 (86%)	0.190	0.33
80 mM CTAB	1.4 (68%)	2.7 (32%)	0.120	0.33
80 mM CTAB + 100 mM caffeine	1.7 (14%)	6.9 (86%)	0.190	0.32

TABLE XIII  
THE LIFETIME COMPONENTS OF ETHIDIUM (Et) IN AQUEOUS SOLVENT AND IN MICELLAR COMPARTMENTS WITH AND WITHOUT CAFFEINE:  $\tau$  REPRESENTS THE TIME CONSTANT IN NS AND THE FIGURES IN THE PARENTHESES REPRESENT RELATIVE CONTRIBUTION OF THE COMPONENT. SURFACTANT AS WELL AS CAFFEINE CONCENTRATIONS MAINTAINED AT 100 MM. ERROR  $\pm 5\%$

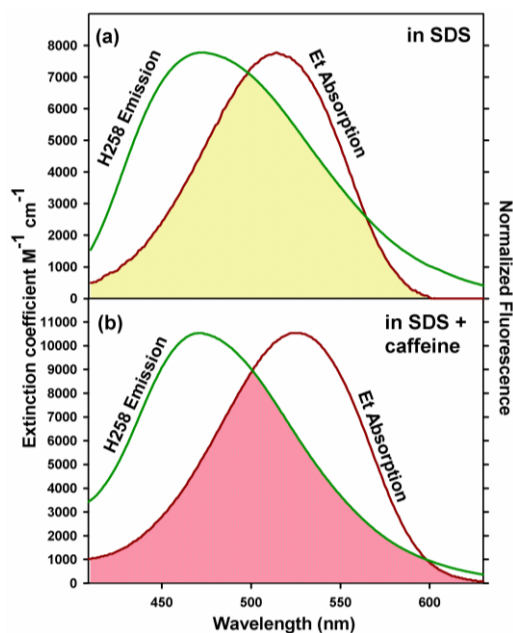
Et in CTAB	1.4 (51%)	2.46 (49%)
Et in CTAB + caffeine	1.9 (14%)	7.2 (86%)
Et in SDS	1.46 (5%)	5.15 (95%)
Et in SDS + caffeine	2.06 (12%)	7.25 (88%)
Et in TX-100	1.21 (16%)	5.37 (84%)
Et in TX-100 + caffeine	1.45 (10%)	6.77 (90%)

Upon addition of caffeine in solution the fluorescence decay becomes faster apparently revealing closer association of H258 and Et (1.94 nm). Relative enhancement of the Et emission (steady state) in H258 coated SDS micelles in presence of caffeine (inset Fig. 24(a)) is also in the favour of the above conclusion.

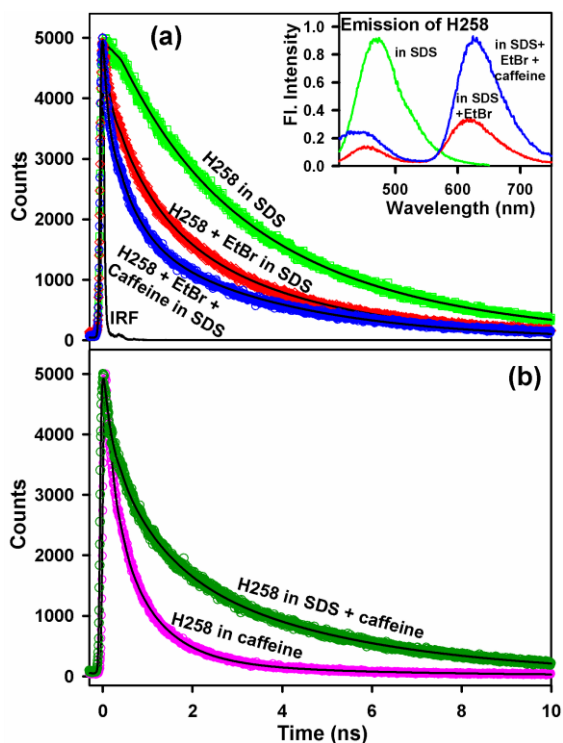
However, upon the addition of caffeine, FRET between H258 and Et is interrupted as Et is released from the micelles in presence of caffeine and such interruption results in the increase in the fluorescence intensity of H258 band. As shown in Fig. 24(b) and Table XVI, fluorescence decay of H258 in the micelles becomes faster upon addition of caffeine as a consequence of partial detachment of H258 from the micellar surface.

Thus, the fate of the H258-Et complex upon addition of caffeine is found to be inconclusive from the standard FRET analysis. We have repeated our experiment with another donor coumarin 500 (C500) which does not interact with caffeine at high temperature ( $\sim 70^\circ\text{C}$ ) as has been reported by our earlier studies[36], however, both caffeine dimer as well as caffeine-Et complex has been

reported by us to be stable even at high temperatures at around 70°C[22].



Figs. 23. The spectral overlap of H258 emission and Et absorption in (a) 20 mM SDS in absence and (b) presence of 100 mM caffeine. (Reprinted with permission from ref.[71]. Copyright 2012, American Chemical Society)



Figs. 24. The temporal decay of H258 (0.2 μM), H258-Et ([Et] = 155 μM) and H258-Et-caffeine ([caffeine] = 100 mM) in (a) 20 mM SDS and that of H258-caffeine in (b) SDS and water. The emission spectra of H258, H258-Et and H258-Et-caffeine in (inset (a)) SDS. All the samples are excited at  $\lambda_{ex} = 375$  nm and fluorescence transients monitored at  $\lambda_{em} = 470$  nm. (Reprinted with permission from ref.[71]. Copyright 2012, American Chemical Society)

TABLE XIV

THE FLUORESCENCE LIFETIME COMPONENTS  $\tau_1$  AND  $\tau_2$  REPRESENT FLUORESCENCE LIFETIMES OF THE SAMPLE WHILE  $\tau_{R1}$  AND  $\tau_{R2}$  REPRESENT ROTATIONAL RELAXATION TIME CONSTANTS OF THE SAME AND  $R_0$  DEFINES ANISOTROPY AT TIME T=0. FIGURES IN PARENTHESES SHOW RELATIVE CONTRIBUTION. ERROR  $\pm 5\%$

Et in	$\tau_1$ (ns)	$\tau_2$ (ns)	Fluorescence anisotropy		
			$\tau_{R1}$ (ns)	$\tau_{R2}$	$r_0$
water	1.6 (100%)		0.110		0.24
100 mM caffeine	2.3 (15%)	7.0 (85%)	0.210		0.23
2 mM SDS	1.6 (89%)	0.08(11%)	0.070 (100%)		0.38
2 mM SDS + 100 mM caffeine	1.7 (11%)	6.6 (89%)	0.180 (100%)		0.31
4 mM SDS	1.8 (83%)	0.13 (17%)	0.09 (100%)		0.37
4 mM SDS + 100 mM caffeine	1.8 (13%)	6.8 (87%)	0.18 (100%)		0.29
6 mM SDS	2.4 (87%)	0.64 (13%)	0.28 (100%)		0.23
6 mM SDS + 100 mM caffeine	1.2 (6%)	6.1 (94%)	0.18 (100%)		0.29
10 mM SDS	1.1 (5%)	4.7 (95%)	1.0 (57%)	0.09 (43%)	0.27
10 mM SDS + 100 mM caffeine	1.3 (6%)	6.4 (94%)	1.6 (47%)	0.19 (53%)	0.25
20 mM SDS	1.4 (9%)	4.7 (91%)	3.4 (34%)	0.39 (66%)	0.24
20 mM SDS + 100 mM caffeine	1.5 (8%)	6.4 (92%)	1.3 (46%)	0.08 (54%)	0.32
40 mM SDS	1.4 (10%)	4.8 (90%)	2.3 (40%)	0.36 (60%)	0.19
40 mM SDS + 100 mM caffeine	1.7 (10%)	6.5 (90%)	2.1 (46%)	0.22(54%)	0.29
80 mM SDS	1.4 (9%)	4.8 (91%)	2.2 (42%)	0.38 (58%)	0.27
80 mM SDS + 100 mM caffeine	1.6 (10%)	6.3 (90%)	2.9 (37%)	0.39 (63%)	0.33
100 mM SDS	1.4 (9%)	4.8 (91%)	1.9 (44%)	0.23 (56%)	0.22
100 mM SDS + 100 mM caffeine	1.5 (9%)	6.2 (91%)	2.9 (43%)	0.35 (57%)	0.32

Hence, we repeated the experiments with the donor coumarin 500 (C500) at 70°C (Figs. 25 and 26, Table XVII) and found that in absence of caffeine 33% donor molecules participate in FRET with 87% energy transfer efficiency (E) whereas in presence of caffeine only 19% donor molecules participate in FRET with E as 80% which is due to the caffeine mediated release of acceptor Et molecules from the SDS micelles.

The donor-acceptor distance (r) also increases from 2.89 nm to 3.16 nm in presence of caffeine.

### III.3.2. Application of Kinetic Models in the Investigation of Caffeine Mediated Dissociation of Et from SDS Micelles

For better understanding of the fate of the association between H258 and Et in presence of caffeine, it is

essential to know the distribution of Et molecules around the micelles before and after the addition of caffeine, because this is a governing factor for efficient energy transfer. The decay of excited probes in a micelle may be described by the following kinetic model, which is known as the Infelta-Tachiya model [74]-[75]:



where  $P_n^*$  stands for a micelle containing an excited probe and  $n$  quencher molecules, while  $P_n$  stands for a micelle which contains  $n$  quencher molecules but no excited probe.  $k_0$  is the total decay constant of the excited state in absence of a quencher.  $k_q$  is the rate constant for quenching of an excited probe in a micelle containing one quencher molecule.

TABLE XV

THE FLUORESCENCE LIFETIME COMPONENTS  $\tau_1$  AND  $\tau_2$  REPRESENT FLUORESCENCE LIFETIMES OF THE SAMPLE WHILE  $\tau_{R1}$  AND  $\tau_{R2}$  REPRESENT ROTATIONAL RELAXATION TIME CONSTANTS OF THE SAME AND  $R_0$  DEFINES ANISOTROPY AT TIME T=0. FIGURES IN PARENTHESES SHOW RELATIVE CONTRIBUTION. ERROR  $\pm 5\%$

Et in	$\tau_1$ (ns)	$\tau_2$ (ns)	Fluorescence anisotropy		
			$\tau_{r1}$ (ns)	$\tau_{r2}$ (ns)	$r_0$
water	1.6 (100%)		0.110		0.24
100 mM caffeine	2.3 (15%)	7.0 (85%)	0.210		0.23
0.1 mM TX-100	1.6 (100%)		0.108		0.35
0.1 mM TX-100 + 100 mM caffeine	2.0 (16%)	7.0 (84%)	0.175		0.36
1 mM TX-100	1.6 (100%)		0.103		0.33
1 mM TX-100 + 100 mM caffeine	1.9 (15%)	6.9 (85%)	0.196		0.30
100 mM TX-100	1.1 (16%)	4.5 (84%)	0.053 (81%)	1.51 (19%)	0.38
100 mM TX-100 + 100 mM caffeine	1.6 (15%)	6.5 (85%)	0.08 (80%)	1.17 (20%)	0.37

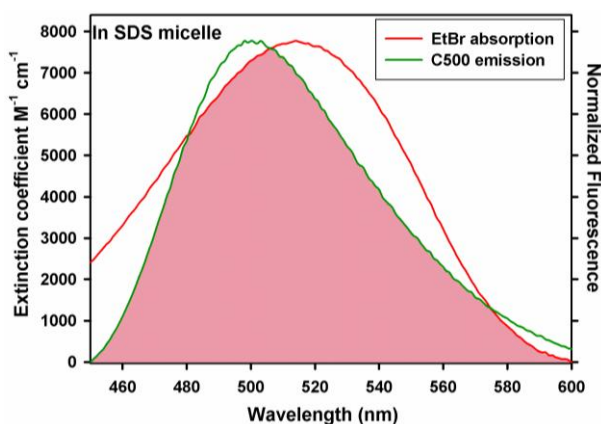


Fig. 25. The spectral overlap of C500 emission and Et absorption in (a) 20 mM SDS (at 70°C). (Reprinted with permission from ref.[71]. Copyright 2012, American Chemical Society)

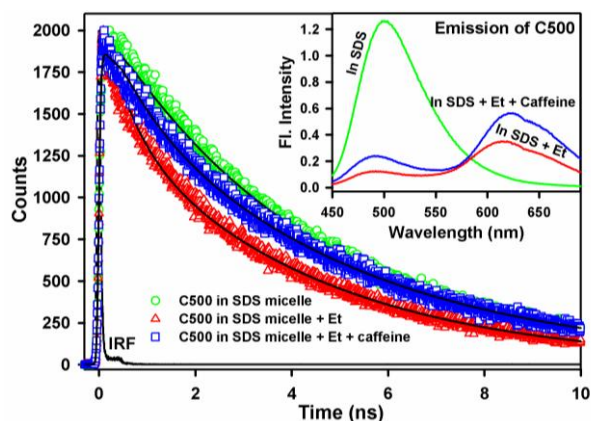


Fig. 26. The temporal decay of C500 in SDS micelles at 70°C in presence and absence of acceptor Et ([Et] = 155  $\mu$ M) and caffeine ([caffeine] = 100 mM) in 20 mM SDS. The corresponding emission spectra are given in inset. (Reprinted with permission from ref.[71]. Copyright 2012, American Chemical Society)

TABLE XVI

THE LIFETIME COMPONENTS OF H258 IN VARIOUS ENVIRONMENTS:  $\tau$  REPRESENTS THE TIME CONSTANT IN NS AND THE FIGURES IN THE PARENTHESES REPRESENT RELATIVE CONTRIBUTION OF THE COMPONENT. [H258] = 0.2  $\mu$ M, [SDS] = 20 MM, [ET] = 155  $\mu$ M AND [CAFFEINE] = 100 MM. ERROR  $\pm 5\%$

Sample	$\tau_1$ (ns)	$\tau_2$ (ns)	$\tau_3$ (ns)
H258 in SDS	3.38 (100%)		
H258 in SDS + Et	3.38 (81%)	0.87 (17%)	0.1 (2%)
H258 in SDS + Et + caffeine	3.38 (80%)	0.55 (17%)	0.08 (3%)
H258 in SDS + caffeine	3.38 (91%)	0.36 (9%)	
H258 in water	3.82 (95%)	0.14 (5%)	
H258 in water + Et	3.82 (69%)	0.49 (21%)	0.09 (10%)
H258 in water + Et + caffeine	3.82 (34%)	0.14 (13%)	0.78 (53%)
H258 in water + caffeine	3.82 (31%)	0.81 (55%)	0.16 (14%)

Thus when micelle containing a probe with  $n$  quencher molecules is excited, the rate constant for the excited state decay of that probe is given by  $k_0 + nk_q$  and the total energy transfer rate constant is  $nk_q$ .

In this kinetic model, it is assumed that the distribution of the number of quenchers attached to one micelle follows a Poisson distribution,[74] namely:

$$p(n) = \left( \frac{m^n}{n!} \right) \exp(-m) \quad (27)$$

where  $m$  is the mean number of quenchers in a micelle:

$$m = k_+ [A] / k_- \quad (28)$$

where  $k_+$  is the rate constant for entry of a quencher molecule into a micelle, while  $k_-$  is the rate constant for exit of a quencher molecule from a micelle containing one quencher molecule.  $A$  stands for a quencher molecule in the aqueous phase. Based upon the above model, the equation for the total concentration  $P^*(t)$  of excited probes at time  $t$  is given by the following Eq. (29)[76]:

$$P^*(t) = P^*(0) \exp \left[ - \left( k_0 + \frac{k_0 k_+ [A]}{k_- + k_q} \right) t - \frac{k_q^2 k_+ [A]}{k_- (k_- + k_q)^2} \left\{ 1 - \exp \left[ - (k_- + k_q) t \right] \right\} \right]$$

If  $k$  is much smaller than  $k_q$ , Eq. (29) reduces to:

$$P^*(t) = P^*(0) \exp \left\{ -k_0 t - m \left[ 1 - \exp(-k_q t) \right] \right\} \quad (30)$$

In one of our systems, along with the Et quencher molecules, there exist some caffeine molecules that also causes quenching of the lifetime of the excited probe (H258) due to its partial release from the micelle and these are also taken into account.

TABLE XVII  
THE LIFETIME COMPONENTS OF C500 AT 70°C IN VARIOUS ENVIRONMENTS:  $\tau$  REPRESENT THE TIME CONSTANTS IN NS AND THE FIGURES IN THE PARENTHESIS REPRESENT RELATIVE CONTRIBUTION OF THE COMPONENTS. ERROR  $\pm 5\%$

Sample	$\tau_1$ (ns)	$\tau_2$ (ns)
C500 in SDS	4.33 (100%)	
C500 in SDS + Et	4.33 (67%)	0.56 (33%)
C500 in SDS + Et + caffeine	4.33 (81%)	0.84 (19%)
C500 in SDS + caffeine	4.33 (100%)	
C500 in water	3.34 (100%)	

If the distribution of the number of caffeine mediated detached donor molecules from the micellar surface follows Poisson distribution with the average number ( $m_c$ ), the decay curve of the excited state of H258 in micelle in presence of caffeine without and with the Et molecules are described by [77]:

$$P^*(t) = P^*(0) \exp \left\{ -k_0 t - m_c \left[ 1 - \exp(-k_{qc} t) \right] \right\} \quad (31)$$

$$P^*(t) = P^*(0) \exp \left\{ -k_0 t - m_c \left[ 1 - \exp(-k_{qc} t) \right] + m \left[ 1 - \exp(-k_q t) \right] \right\} \quad (32)$$

where the quenching rate constant ( $k_{qc}$ ) by caffeine molecules may be different from that ( $k_q$ ) by Et molecules. We have determined the values of the parameters  $m_c$ ,  $k_{qc}$ ,  $k_0$ ,  $m$ , and  $k_q$  by fitting the equations (30), (31) and (32) to the decay curves in the absence and presence Et and caffeine molecules (Fig. 27 and Table XIII).

We have also employed extended Infelta-Tachiya kinetic model described by the following equation [78]:

$$P^*(t) = P^*(0) \exp \left[ -\gamma t + \mu \left( \exp^{-\beta t} - 1 \right) \right] \quad (33)$$

where  $\gamma$ ,  $\mu$ , and  $\beta$  are functions of the rate constants of probe migration ( $k$ ), quenching ( $k_q$ ), and quencher exchange either by micelle collision ( $k_e$ ) or via the aqueous phase ( $k$ ) and are explicitly defined as:

$$\gamma = k_0 + k + m a_2 k_q / \beta \quad (34)$$

$$\mu = m k_q^2 / \beta^2 \quad (35)$$

$$\beta = k_q + a_2 \quad (36)$$

$$a_2 = k_e [M] + k_- \quad (37)$$

In the expressions (34)-(37),  $k_0$ ,  $m$  and  $[M]$  stand for the deactivation rate constant of the excited probe in absence of quencher, the average number of quenchers per micelle, and the micelle concentration, respectively. The quenching parameters  $k_0$ ,  $m$ , and  $k_q$  derived from the extended Infelta-Tachiya model (Fig. 27 inset and Table XIX) found to be comparable with those derived from the generalized version of Infelta-Tachiya model.

Fig. 27 shows the time resolved fluorescence transients of H258 in absence and presence of caffeine and Et molecules, fitted with Eqs. (30), (31) and (32) whereas Fig. 27 inset shows the same fitted with Eq. (33). The observed fluorescence transients were fitted using a nonlinear least squares fitting procedure (software SCIENTIST™) to a function  $\left( X(t) = \int_0^t E(t') P(t-t') dt' \right)$  comprising of the convolution of the instrument response function (IRF) ( $E(t)$ ) with exponential:

$$\left\{ P(t) = P(0) \exp \left\{ -k_0 t - m_c \left[ 1 - \exp(-k_{qc} t) \right] + m \left[ 1 - \exp(-k_q t) \right] \right\} \right\}$$

The purpose of this fitting is to obtain the decays in an analytic form suitable for further data analysis. As evident from the figure, the models describe the decay curves reasonably well.

The quenching parameters are summarized in Table XIII and Table XIX. Upon fitting the decay curves of H258 with the kinetic models mentioned before, it is clear that the distribution of Et molecules on the micellar surface changes significantly after the addition of caffeine. As summarized in Table XIII and Table XIX, the mean number of Et molecules associated with the micelle ( $m$ ) reduces after the addition of caffeine.

Thus caffeine shows efficiency in the detachment of Et from the micellar surface. The quenching rate constant ( $k_q$ ) due to the acceptor (Et) molecules increases in presence of caffeine revealing closer association between the remaining Et and H258 molecules on the micellar surface which is consistent with the results obtained from

FRET study and steady state emission spectroscopy as mentioned before. However, standard FRET analysis failed to monitor the detachment of the bound Et molecules from the micellar surface in presence of caffeine quantitatively. We have also employed Infelta-Tachiya model on our FRET study using C500 as the donor which does not interact with caffeine molecules at the experimental conditions [36] (Fig. 28 and Table XX). The results clearly show decrease in the mean number of Et molecules associated with the micelle upon addition of caffeine due to the caffeine mediated release of Et from the SDS micelle. Furthermore, we determine the equilibrium constant for solubilization of Et in SDS micelles before and after the addition of caffeine. The total concentrations  $[M]$  and  $[Q]$  of micelles and Et introduced in solution are related through the following equation:

$$m[M] + [A] = [Q] \quad (38)$$

$$m = k_+ [A] / k_- \quad (39)$$

where  $[A]$  is the concentration of Et in the aqueous phase. Elimination of  $[A]$  from Eqs. (38) and (39) yields:

$$K_{eq} = k_+ / k_- = m / ([Q] - m[M]) \quad (40)$$

where  $K_{eq}$  is the equilibrium constant ( $k_+/k_-$ ) for the solubilization of Et in micelles and calculated to be  $2.3 \times 10^4$  and  $3.3 \times 10^3 \text{ M}^{-1}$  in absence and presence of caffeine respectively.  $K$  has been calculated for different concentrations of Et in absence of caffeine and has been found to be similar.

The significant decrease in the value of equilibrium constant ( $K_{eq}$ ) for solubilization of Et in micelles upon addition of caffeine confirms the efficacy of caffeine molecules in the detachment of Et from the biomimetic systems like micelles.

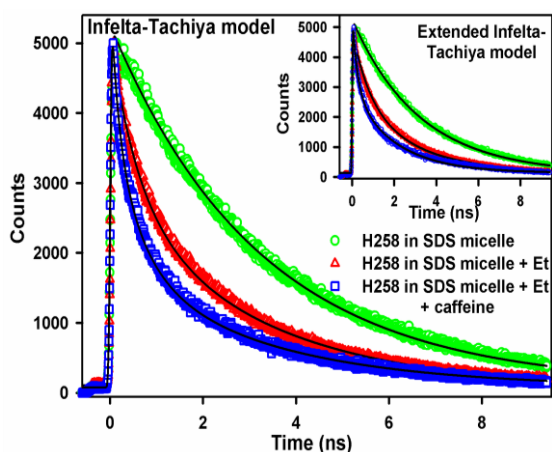


Fig. 27. Time resolved fluorescence decay curves of H258 in SDS micelles in absence and presence of caffeine and Et. The bold lines represent the fitting of the curves by the generalized version as well as the extended version (inset) of the kinetic models developed by Infelta and Tachiya (see text). (Reprinted with permission from ref.[71]. Copyright 2012, American Chemical Society)

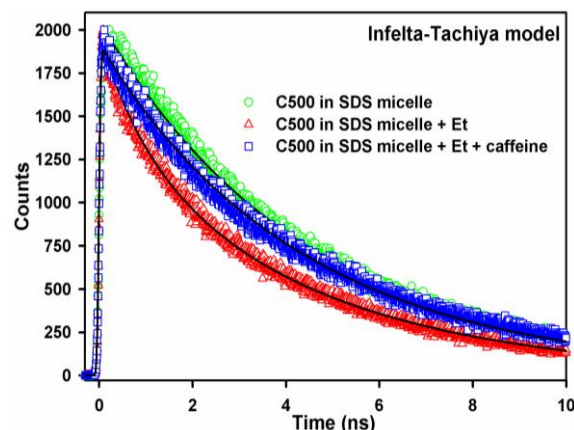


Fig. 28. Time resolved fluorescence decay curves of H258 in SDS micelles in absence and presence of caffeine and Et. The bold lines represent the fitting of the curves by the generalised version of the kinetic models developed by Infelta and Tachiya. (Reprinted with permission from ref.[71]. Copyright 2012, American Chemical Society)

TABLE XIII  
VALUES OF THE QUENCHING PARAMETERS USING THE SIMPLIFIED VERSION OF THE MODEL DEVELOPED BY INFELTA-TACHIYA

System	$k_0$ (ns <sup>-1</sup> )	$m$	$k_q$ (ns <sup>-1</sup> )	$m_c$	$k_{qc}$ (ns <sup>-1</sup> )
Micelle bound H258	0.31	-	-	-	-
Micelle bound H258 + Et	0.31	0.66	1.08	-	-
Micelle bound H258 + Et + caffeine	0.31	0.31	5.34	0.89	1.11

TABLE XIX  
VALUES OF THE QUENCHING PARAMETERS USING THE EXTENDED VERSION OF THE MODEL DEVELOPED BY INFELTA-TACHIYA

System	$k_0$ (ns <sup>-1</sup> )	$k$ (ns <sup>-1</sup> )	$m$	$k_q$ (ns <sup>-1</sup> )
Micelle bound H258	0.31	-	-	-
Micelle bound H258 + Et	0.31	-	0.82	0.57
Micelle bound H258 + Et + caffeine	0.31	0.17	0.69	2.92

TABLE XX  
VALUES OF THE QUENCHING PARAMETERS USING THE SIMPLIFIED VERSION OF THE MODEL DEVELOPED BY INFELTA-TACHIYA: ERROR  $\pm 5\%$

System	$k_0$	$m$	$k_q$
Micelle bound C500	0.23	-	-
Micelle bound C500 + Et	0.23	0.35	0.70
Micelle bound C500 + Et + caffeine	0.23	0.02	0.70

### III.3.3. Interruption in FRET due to Caffeine Mediated Expulsion of Et from Epithelial Cells: a Fluorescence Microscopic View

Significant perturbation of FRET efficiency from the donor H258 to the acceptor Et has been revealed even from our cellular studies. Fig. 29 shows the fluorescence micrographs of the squamous epithelial cells stained with both the donor (H258) and the acceptor (Et) fluorophores.

The donor emits in the blue region of the visible spectrum (Fig. 23) whereas the acceptor emits in the red region of the same. H258 and Et, being well known DNA minor groove binder[79] and DNA intercalator[35],[66] respectively, and both being cell permeable[22],[80],

stain the nuclei of the cells. Upon specifically exciting the donor dye molecules under UV light at 360 nm we observe only the red (acceptor) emission from the nuclei of the cells, which emphasizes the FRET from the donor to the acceptor.

However, as shown in Fig. 29, upon the addition of caffeine (+ caffeine), we find the red emission from the acceptor changes to the blue emission of the donor with time, showing significant perturbation in the FRET efficiency between the two.

Photobleaching of the donor (H258) and acceptor (Et) molecules both in absence and presence of caffeine have been monitored by us in our control studies (data not shown) where we find no signature of acceptor photobleaching both in absence and presence of caffeine within the experimental time frame. Donor H258 molecules also do not undergo photobleaching in presence of caffeine but significant photobleaching of the donor molecules in absence of caffeine has been observed.

It has to be noted that the emission intensity of the donor even after 800 seconds of caffeine treatment is less than that in absence of the acceptor (image not shown) most probably due to the fraction of acceptor molecules that still remained associated with the DNA in the nuclei even after the addition of caffeine.

Possibility of removal of some of the donor molecules from the nucleus cannot be ruled out. Whereas, in the control experiment, in which the cells were treated only with the phosphate buffer saline (PBS) without caffeine (- caffeine), we find no significant change in the red emission from the nuclei with time.

To highlight the observed perturbation in FRET efficiency from H258 to Et in presence of caffeine in a more quantitative manner, the average intensity of the red (acceptor) and blue (donor) emission from the nuclei in each micrograph has been plotted against time for both test (+ caffeine) and control (- caffeine) experiments as shown in Figs. 30(a) and (b), respectively. In Fig. 30(a), the drop in emission intensity of the acceptor with time has been fitted biexponentially (within  $\pm 10\%$  error) with the characteristic time constants of 122 and 550 seconds, which exactly coincides with that of the biexponential fit of the rise of the donor emission intensity with time within the error limit.

As shown in Fig. 30(b), in control experiment (- caffeine) there is a slight decrease in the red emission intensity of the acceptor due to the partial detachment of Et from the cell nuclei by the PBS buffer which leads to the slight increase in the blue emission intensity of the donor. As we observe slight increase in the blue fluorescence intensity of the donor it can be concluded that the donor H258 molecules undergo photobleaching at a much slower rate compared to the buffer mediated release of non-specifically bound EtBr.

The respective decay and rise of the acceptor and donor can be fitted single exponentially within the same error limit with a characteristic time component of 550 seconds, which coincides with the slower time

component obtained in presence of caffeine. Thus this slower time component of 550 seconds can be assigned to the caffeine independent release of Et from the cell nuclei by the buffer itself and the faster time component (122 second) is achieved solely due to the presence of caffeine.

Therefore, the caffeine-mediated release of the bound Et from cell nuclei is almost 5 times faster compared to the solvent alone.

It has to be noted that the time constant for the release of Et from the nuclei of squamous epithelial cells reported here, is much slower than that proposed in our earlier work[22], which accounts for the lower caffeine concentration purposely used in our present work to vividly show the alteration of FRET.

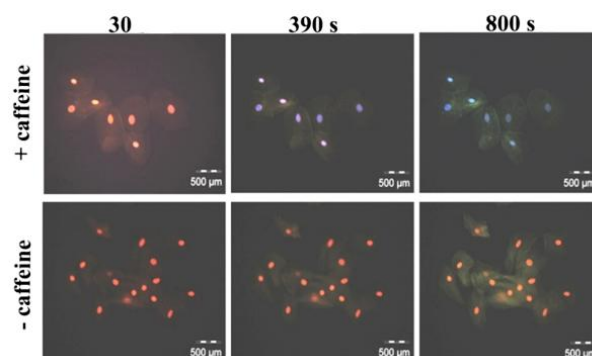


Fig. 29. Fluorescence micrographs of squamous epithelial cells doubly stained with H258 and Et after 30, 390 and 800 seconds upon treatment with caffeine (+ caffeine) along with the control sets (- caffeine) treated with PBS without caffeine. (Reprinted with permission from ref.[71]. Copyright 2012, American Chemical Society)

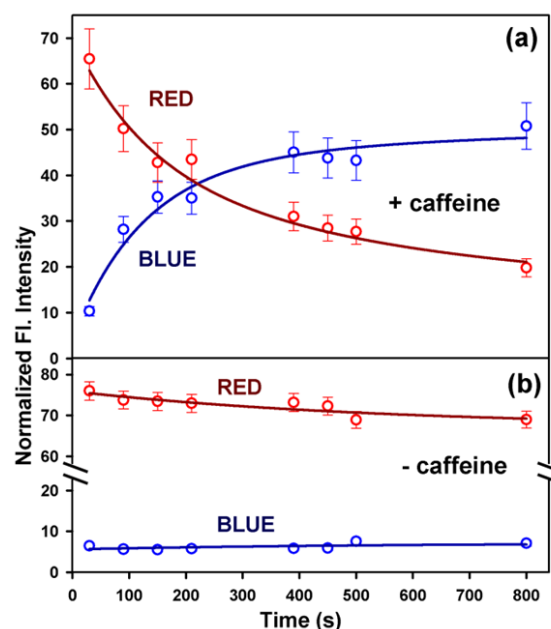


Fig. 30. Rate of change in the intensity of red and blue emission from the doubly stained squamous epithelial cells (a) upon treatment with caffeine (+ caffeine) and (b) upon treatment with PBS without caffeine (- caffeine) taken as control. (Reprinted with permission from ref.[71]. Copyright 2012, American Chemical Society)

#### IV. Conclusion

In the present study we have exploited the dimeric nature of caffeine to host some hydrophobic molecules like DCM, C500 and TNS. The results of the molecular modeling calculations provide a mechanistic model of confinement of such molecules within the caffeine dimer that is consistent with the *in vitro* studies involving NMR experiments. We have explored the hydration dynamics associated with caffeine dimer, which plays a key role in the biomolecular recognition of such xanthine alkaloids. The DLS studies associated with FTIR, sonometric, densimetric and steady state optical experiments clearly reveal the dimeric nature of the caffeine molecules in aqueous solution which is consistent with the previously reported studies. While the sonometric/densimetric studies explore the static picture of hydration around the caffeine dimers, picosecond/femtosecond resolved experiments demonstrate the key time scales associated with the dynamics of hydration. The femtosecond resolved fluorescence study at 80°C reveals solvation of the probe with time scales of 0.6 ps and 5.85 ps, which are slower than that in bulk water but faster than micelles or reverse micelles confirming the weakly structured nature of the hydrated water molecules. The dynamics of water molecules as revealed by C500 show solvation time scale of 0.3 and 0.7 ps at room temperature and it reduces to 0.3 ps at 55°C. In presence of a large ion like guanidium hydrochloride the process becomes slower with time constants of 0.5 and 2.1 ps at room temperature and 0.8 ps at 55°C. All these time scales are however, faster than those observed for caffeine solutions even at elevated temperature confirming the structured nature of the hydrated water molecules in caffeine solution with respect to an ionic solution.

Our polarization gated picosecond resolved experiment on the confined DCM and TNS in the caffeine dimer at various temperature explores the activation energy ( $E^*$ ) for the viscous flow and has been found to be comparable to that of bulk water, which further suggests that very weakly structured water molecules are associated with the caffeine dimers. Very slow water dynamics being a characteristic of strongly bonded water molecules, would have prevented the interaction of such xanthine alkaloids with biomolecules whereas very fast dynamical nature of bound water would not have allowed the formation of caffeine dimer itself. The observed dynamical nature of water molecules associated with caffeine dimer makes it a suitable subject for biomolecular interaction where the bound water molecules can be displaced in presence of its receptor molecule facilitating the hydrophobic interaction. Our observations may find the relevance in the exploration of such biomolecular recognition of the most widely consumed caffeine molecules in physiologically relevant environments. Furthermore our exploration of TICT dynamics of TNS in presence of caffeine gives us an idea about the amount of energy required to release such model drugs from the caffeine bound state and this may find significance in further investigation of the use of

such xanthine alkaloids as a tool for targeted drug delivery.

Furthermore, our steady state and time resolved fluorescence studies with synthetic DNA emphasize the interceptive role of well consumed caffeine molecules, forming heterocomplexes with Et. Temperature dependent pico-second resolved fluorescence experiments highlight the thermal stability of such complexes within and beyond the physiological temperature. Results from NMR and DLS studies were used to construct a model of caffeine-Et dimer representing the dominant structure of Et:caffeine complex in solution.

Our cellular studies reveal the precise nature of the xanthine alkaloid in the exclusion of mutagenic Et from the cell nucleus. The specific molecular interaction of caffeine with Et molecule underlying the “interceptor” action of caffeine can be considered as one of the potential mechanism of Et release in our present study. For the physiological activity of the drugs in presence of caffeine another mechanism of action called “protector”, can also occur, in which there is a competition between caffeine and Et for the binding sites on DNA. It is likely that both mechanisms can act simultaneously and therefore must be taken into consideration when analysing a three-component equilibrium of the Et, caffeine and DNA. We believe that our studies may find relevance in the therapeutic use of caffeine as the non-invasive antimutagenic agent particularly for the prevention of oral cancers / squamous cell carcinomas which arises due to the activation of oncogenes as a result of DNA mutation.

In addition, our study finds caffeine as an efficient drug for the removal of a model DNA-intercalator Et from both negatively charged SDS and positively charged CTAB micelles without or with negligible perturbation of their structural integrity. However, caffeine fails to show such activity in case of neutral (polar) TX-100 micelles.

The FRET study focuses on the efficacy of caffeine molecules in altering the association between two DNA binding ligands H258 and Et residing on a micellar surface. However, in our system, standard FRET fails to provide an explicit picture of such alteration in the association between the two DNA-binding ligands on the biomimetic system in presence of caffeine. Our analysis of the experimental results employing the well established kinetic model developed by Infelta and Tachiya, helps to recognize the efficacy of caffeine molecules in the detachment of Et from the biomimetic system.

The result of our cellular studies further emphasizes on the perturbation of FRET efficiency from H258 to Et in presence of caffeine. Our study may help to carry out further experiments in the fields of medicine where caffeine can be taken as an active ingredient to protect cells from various cell damaging agents like DNA-intercalators.

## Acknowledgements

S.B thanks UGC India, for providing research fellowship. We thank DST, India, for financial grant (SR/SO/BB- 15/2007). We thank colleagues in our laboratory at S.N. Bose National Centre for Basic Sciences, whose contributions over the years, acknowledged in the references, have been priceless in the successful evolution of work in this area. In particular, we thank Dr. Pramod Kumar Verma and Dr. Rajib Kumar Mitra. We thank Prof. Gautam Basu, Bose Institute, Kolkata (India), Dr. Anirban Sidhanta & Mr. Debajit Bhowmik, Calcutta University, Kolkata (India) and Prof Masanori Tachiya, Advanced Industrial Science and Technology (AIST), Tsukuba (Japan) for the collaborative work.

## References

- [1] Selby, C. P., Sancar, A., Molecular mechanisms of DNA repair inhibition by caffeine, *Proc. Natl. Acad. Sci.*, volume 87, (issue 9), May 1990, pages 3522-3525.
- [2] Larsen, R. W., Jasuja, R. *et al.*, Spectroscopic and molecular modelling studies of caffeine complexes with DNA intercalators, *Biophys. J.*, volume 70, (issue 1), January 1996 pages 443-452.
- [3] Davies, D. B., Veselkov, D. A. *et al.*, Heteroassociation of caffeine and aromatic drugs and their competitive binding with a DNA oligomer., *Eur Biophys J.*, volume 30, (issue 5), september 2001, pages 354-366.
- [4] McKelvey, V. J., McKenna, P. G., Enhanced synergism between caffeine and mitomycin C in the induction of cytogenetic aberrations in thymidine kinase-deficient Friend murine erythroleukaemia cells *Mutagenesis*, volume 1, (issue 3), May 1986, pages 173-178
- [5] Mourelatos, D., Dozi-Vassiliades, J. *et al.*, Enhancement of Cytogenetic Damage and of Antineoplastic Effect by Caffeine in Ehrlich Ascites Tumor Cells Treated with Cyclophosphamide in Vivo, *Cancer Res*, volume 48, (issue 5), March 1988, pages 1129-1131.
- [6] Ross, W. E., Zwelling, L. A. *et al.*, Relationship between cytotoxicity and dna strand break-age produced by adriamycin and other intercalating agents, *Int. J. Radiat. Oncol. Biol. Phys.*, volume 5, (issue 6), August 1979, pages 1221-1224.
- [7] Iliakis, G., Nusse, M. *et al.*, Differential reduction by caffeine of adriamycin induced cell killing and cell cycle delays in chinese hamster v79 cells, *Int. J. Radiat. Oncol. Biol. Phys.*, volume 12, (issue 11), November 1986, pages 1987-1995.
- [8] Ganapathi, R., Grabowski, D. *et al.*, Modulation of Adriamycin and N-Trifluoroacetyladiamycin-14-valerate Induced Effects on Cell Cycle Traverse and Cytotoxicity in P388 Mouse Leukemia Cells by Caffeine and the Calmodulin Inhibitor Trifluoperazine, *Cancer Res.*, volume 46, (issue 11), November 1986, pages 5553-5557.
- [9] Traganos, F., Kaminska-Eddy, B. *et al.*, Caffeine reverses the cytotoxic and cell kinetic effects of Novantrone (mitoxantrone), *Cell Prolif.*, volume 24, (issue 3), May 1991, pages 305-319.
- [10] Johansson, B., Halldner, L. *et al.*, Hyperalgesia, anxiety, and decreased hypoxic neuroprotection in mice lacking the adenosine A 1 receptor, *Proc. Natl. Acad. Sci.*, volume 98, (issue 16), July 2001, pages 9407-9412.
- [11] Danilov, V. I., Shestopalova, A. V., Hydrophobic effect in Biological Associates: A Monte Carlo Simulation of Caffeine Molecules Stacking, *Int. J. Quantum Chem*, volume 35, (issue 1), January 1989, pages 103-112.
- [12] Wong, E. L. S., Gooding, J. J., The Electrochemical Monitoring of the Perturbation of Charge Transfer through DNA by Cisplatin, *J. Am. Chem. Soc.*, volume 129, (issue 29), June 2007, pages 8950-8951.
- [13] Řeha, D., Kabelá, M. *et al.*, Intercalators. 1. Nature of Stacking Interactions between Intercalators (Ethidium, Daunomycin, Ellipticine, and 4',6-Diaminide-2-phenylindole) and DNA Base Pairs. Ab Initio Quantum Chemical, Density Functional Theory, and Empirical Potential Study, *J. Am. Chem. Soc.*, volume 124, (issue 13), March 2002, pages 3366-3376.
- [14] Rips, I., Jortner, J., Dynamic solvent effects on outer-sphere electron transfer, *J. Chem. Phys.*, volume 87, (issue 4), August 1987, pages 2090-2104.
- [15] Hynes, J. T., Outer-sphere electron-transfer reactions and frequency-dependent friction, *J. Phys. Chem.*, volume 90, (issue 16), July 1986, pages 3701-3706.
- [16] Traganos, F., Kapuscinski, J. *et al.*, Caffeine modulates the effects of DNA-intercalating drugs in vitro: a flow cytometric and spectrophotometric analysis of caffeine interaction with novantrone, doxorubicin, ellipticine, and the doxorubicin analogue AD198, *Cancer Res.*, volume 51, (issue 14), July 1991, pages 3682-3689.
- [17] Mahler, H. R., Perlman, P. S., Effects of mutagenic treatment by ethidium bromide on cellular and mitochondrial phenotype, *Arch. Biochem. Biophys.*, volume 148, (issue 1), January 1972, pages 115-129.
- [18] Johnson, I. M., Kumar, S. G. B. *et al.*, De-intercalation of Ethidium Bromide and Acridine Orange by Xanthine Derivatives and Their Modulatory Effect on Anticancer Agents: A study of DNA-directed Toxicity Enlightened by Time Correlated Single Photon Counting, *J. Biomol. Struct. Dyn.*, volume 20, (issue 5), May 2003, pages 677-685.
- [19] Kapuscinski, J., Kimmel, M., Thermodynamic model of mixed aggregation of intercalators with caffeine in aqueous solution, *Biophys.Chem.*, volume 46, (issue 2), April 1993, pages 153-163.
- [20] Davies, D. B., Veselkov, D. A. *et al.*, Hetero-association of caffeine and aromatic drugs and their competitive binding with a DNA oligomer, *Eur. Biophys. J.*, volume 30, (issue 5), September 2001, pages 354-366.
- [21] Piosik, J., Zdunek, M. *et al.*, The modulation by xanthines of the DNA-damaging effect of polycyclic aromatic agents: Part II. The stacking complexes of caffeine with doxorubicin and mitoxantrone, *Biochemical Pharmacology.*, volume 63, (issue 4), February 2002, pages 635-646.
- [22] Banerjee, S., Bhowmik, D. *et al.*, Ultrafast Spectroscopic Study on Caffeine Mediated Dissociation of Mutagenic Ethidium from Synthetic DNA and Various Cell Nuclei, *J. Phys. Chem. B.*, volume 115, (issue 49), October 2011, pages 14776-14783.
- [23] Turro, N. J., Grätzel, M. *et al.*, Photophysical and Photochemical Processes in Micellar Systems, *Angew. Chem. Intern. Ed.*, volume 19, (issue 9), September 1980, pages 675-696.
- [24] Zhong, D., Pal, S. K. *et al.*, Femtosecond Studies of Protein -DNA Binding and Dynamics: Histone I, *Chem Phys Chem*, volume 2, (issue 4), April 2001, pages 219 -227.
- [25] Pal, S. K., Peon, J. *et al.*, Biological water at the protein surface: Dynamical solvation probed directly with femtosecond resolution, *Proc. Natl. Acad. Sci.*, volume 99, (issue 4), February 2002, pages 1763-1768.
- [26] Mitra, R. K., Sinha, S. S. *et al.*, Interactions of Nile Blue with Micelles, Reverse Micelles and a Genomic DNA, *J. Fluoresc.*, volume 18, (issue 2), March 2008, pages 423-432.
- [27] Banerjee, D., Pal, S. K., Ultrafast charge transfer and solvation of DNA minor groove binder: Hoechst 33258 in restricted environments, *Chem. Phys. Lett.*, volume 432, (issue 2006), pages 257-262.
- [28] Sitkowski, J., Stefaniak, L. *et al.*, Complete assignments of the 1H, 13C and 15N NMR spectra of caffeine, *Spectrochim. Acta Part A Mol. Biomol. Spectrosc.*, volume 51, (issue 5), May 1995, pages 839-841.
- [29] Connor, D. V. O., Philips, D. *Time Correlated Single Photon Counting*, 1984.
- [30] Philips, L. A., Webb, S. P. *et al.*, High-pressure studies of rotational reorientation dynamics: The role of dielectric friction, *J. Chem. Phys.*, volume 83, (issue 11), December 1985, pages 5810-5821.
- [31] Kalman, B., Clarke, N. *et al.*, Dynamics of a new fluorescent probe, 2,5,8,11-tetra-tert-butylperylene in solution, cubic lyotropic liquid crystals, and model membranes, *J. Phys. Chem.*, volume 93, (issue 11), January 1989, pages 4608-4615.

- [32] Kapusta, P., Erdmann, R. *et al.*, Time-Resolved Fluorescence Anisotropy Measurements Made Simple, *J. Fluoresc.*, volume 13, (issue 2), March 2003, pages 179-183.
- [33] Bockris, J. O. M., Saluja, P. P. S., Ionic Solvation Numbers from Compressibilities and Ionic Vibration Potentials Measurements, *J. Phys. Chem.*, volume 76, (issue 15), July 1972, pages 2140-2151.
- [34] Lakowicz, J. R. *Principles of fluorescence spectroscopy*; Kluwer Academic/Plenum: New York, 1999.
- [35] Banerjee, D., Pal, S. K., Simultaneous Binding of Minor Groove Binder and Intercalator to Dodecamer DNA: Importance of Relative Orientation of Donor and Acceptor in FRET, *J. Phys. Chem. B. (Letter)*, volume 111, (issue 19), April 2007, pages 5047-5052.
- [36] Banerjee, S., Verma, P. K. *et al.*, Probing the interior of Self-assembled Caffeine Dimer at various Temperatures, *J. Fluoresc.*, volume 22, (issue 2), March 2012, pages 753-769.
- [37] Carlucci, L., Gavezzotti, A., Molecular Recognition and Crystal Energy Landscapes: An X-ray and Computational Study of Caffeine and Other Methylxanthines, *Chem. Eur. J.*, volume 11, (issue 1), December 2005, pages 271 - 279.
- [38] Jahagirdar, D. V., Arbad, B. R. *et al.*, Studies in Partial Molar Volumes, Partial Molar Compressibilities and Viscosity B-Coefficients of Caffeine in Water at Four Temperatures., *J. Mol. Liq.*, volume 85, (issue 3), May 2000, pages 361-373.
- [39] Maevsky, A. A., Sukhorukov, B. I., IR study of base stacking interactions *Nucl. Acids Res.*, volume 8, (issue 13), July 1980, pages 3029-3042.
- [40] Millero, F. J., Surdo, A. L. *et al.*, The apparent molal volumes and adiabatic compressibilities of aqueous amino acids at 25.degree.C, *J. Phys. Chem.*, volume 82, (issue 7), April 1978, pages 784-792.
- [41] Benz, R., Some Thermodynamic Properties Of The System PuCl<sub>3</sub>—KCl From Electromotive force data, *J. Phys. Chem.*, volume 65, (issue 1), January 1961, pages 81-84.
- [42] Pal, S. K., Sukul, D. *et al.*, Solvation Dynamics of DCM in Micelles, *Chem. Phys. Lett.*, volume 327, (issue 1-2), September 2000, pages 91-96.
- [43] Sarkar, R., Shaw, A. K. *et al.*, Ultrafast photoinduced deligation and ligation dynamics: DCM in micelle and micelle-enzyme complex, *J. Photochem. Photobiol. B*, volume 83, (issue 3), June 2006, pages 213-222.
- [44] Pal, S. K., Mandal, D. *et al.*, Solvation dynamics of 4-(dicyanomethylene)-2-methyl-6-(p-dimethylaminostyryl)-4H-pyran (DCM) in a microemulsion, *Chem. Phys. Lett.*, volume 312, (issue 2-4), October 1999, pages 178-184.
- [45] Wu, M., Gu, W. *et al.*, Preparation and characterization of ultrafine zinc sulfide particles of quantum confinement, *Chem Phys Lett*, volume 224, (issue 5-6), July 1994, pages 557-562.
- [46] Meulen, P. v. d., Zhang, H. *et al.*, Subpicosecond Solvation Relaxation of 4-(Dicyanomethylene)-2-methyl-6-(p-(dimethylamino)styryl)-4H-pyran in Polar Liquids, *J. Phys. Chem.*, volume 100, (issue 13), March 1996, pages 5367-5373.
- [47] Drake, J. M., Lesiecki, M. L. *et al.*, Photophysics and Cis\_Trans Isomerization of DCM, *Chem Phys Lett*, volume 113, (issue 1985), pages 530-534.
- [48] Zhang, H., Jonkman, A. M. *et al.*, Femtosecond studies of charge separation in photo-excited DCM in liquid solution, *Chem Phys Lett*, volume 224, (issue 5-6), July 1994, pages 551-556.
- [49] Easter, D. C., Baronavski, A. P., Ultrafast relaxation in the fluorescent state of the laser dye DCM, *Chem Phys Lett*, volume 201, (issue 1-4), January 1993, pages 153-158.
- [50] Zana, R., Microviscosity of Aqueous Surfactant Micelles: Effect of Various Parameters, *J. Phys. Chem. B.*, volume 103, (issue 43), July 1999, pages 9117-9125.
- [51] Fee, R. S., Maroncelli, M., Estimating the time-zero spectrum in time-resolved emission measurements of solvation dynamics, *Chem Phys.*, volume 183, (issue 2-3), June 1994, pages 235-247.
- [52] Jimenez, R., Fleming, G. R. *et al.*, Femtosecond solvation dynamics of water, *Nature*, volume 369, (issue 6480), June 1994, pages 471 - 473.
- [53] Riter, R. E., Willard, D. W. *et al.*, Water Immobilization at Surfactant Interfaces in Reverse Micelles, *J. Phys. Chem. B.*, volume 102, (issue 15), March 1998, pages 2705-2714.
- [54] Corbeil, E. M., Levinger, N. E., Dynamics of Polar Solvation in Quaternary Microemulsions, *Langmuir*, volume 19, (issue 18), July 2003, pages 7264-7270.
- [55] Hirose, K., A Practical Guide for the Determination of Binding Constants, *J. Incl. Phenom. Macrocycl. Chem.*, volume 39, (issue 3-4), April 2001, pages 193-209.
- [56] Datta, A., Mandal, D. *et al.*, Interaction of Triton X-100 with cyclodextrins. A fluorescence study, *J. Chem. Soc., Faraday Trans.*, volume 94, (issue 23), 1998, pages 3471-3475.
- [57] Chang, T. L., Cheung, H. C., A model for molecules with twisted intramolecular charge transfer characteristics: solvent polarity effect on the nonradiative rates of dyes in a series of water-ethanol mixed solvents, *Chem. Phys. Lett.*, volume 173, (issue 4), October 1990, pages 343-348.
- [58] Bhattacharyya, K., Chowdhury, M., Environmental and magnetic field effects on exciplex and twisted charge transfer emission, *Chem. Rev.*, volume 93, (issue 1), January 1993, pages 507-535.
- [59] Sarkar, N., Das, K. *et al.*, Interaction of urea with fluorophores bound to cyclodextrins. Fluorescence of p-toluidino naphthalene sulfonate, *Chem. Phys. Lett.*, volume 196, (issue 5), August 1992, pages 491-496.
- [60] Nakamura, A., Saitoh, K. *et al.*, Fluctuation in structure of inclusion complexes of cyclodextrins with fluorescent probes, *Chem. Phys. Lett.*, volume 187, (issue 1-2), November 1991, pages 110-115.
- [61] Sarkar, N., Das, K. *et al.*, Salt effect on the hydrophobic binding of p-toluidino naphthalene sulfonate with cyclodextrins, *Chem. Phys. Lett.*, volume 218, (issue 5-6), February 1994, pages 492-498.
- [62] Almgren, M., Grieser, F. *et al.*, Dynamic and static aspects of solubilization of neutral arenes in ionic micellar solutions, *J. Am. Chem. Soc.*, volume 101, (issue 2), January 1979, pages 279-291.
- [63] Jobe, D. J., Verrall, R. E. *et al.*, Fluorescence and Conductometric Studies of Potassium 2-(p-Toluidinyl)naphthalene-6-sulfonate/Cyclodextrin/Surfactant Systems, *J. Phys. Chem.*, volume 92, (issue 12), June 1988, pages 3582-3586.
- [64] Catena, G. C., Bright, F. V., Thermodynamic Study on the Effects of P-Cyclodextrin Inclusion with Anilino-naphthalenesulfonates, *Anal. Chem.*, volume 61, (issue 8), April 1989, pages 905-909.
- [65] Sen, P., Mukherjee, S. *et al.*, Temperature dependence of solvation dynamics in a micelle. 4-Aminophthalimide in Triton X-100, *Chem. Phys. Lett.*, volume 385, (issue 5-6), February 2004, pages 357-361.
- [66] Sarkar, R., Pal, S. K., Ligand-DNA Interaction in a Nanocage of Reverse Micelle, *Biopolymers*, volume 83, (issue 6), December 2006, pages 675-686.
- [67] Baranovsky, S. F., Bolotin, P. A. *et al.*, Interaction of Ethidium Bromide and Caffeine with DNA in Aqueous Solution, *J. Appl. Spectrosc.*, volume 76, (issue 1), January 2009, pages 132-139.
- [68] Falk, M., Chew, W. *et al.*, Molecular modelling and NMR studies of the caffeine dimer, *Can. J. Chem.*, volume 76, (issue 1), 1998, pages 48-56.
- [69] Ortega, A., Amoros, D. *et al.*, Prediction of hydrodynamic and other solution properties of rigid proteins from atomic and residue-level models, *Biophys. J.*, volume 101, (issue 4), August 2011, pages 892-898.
- [70] Lai, J. S., Herr, W., Ethidium bromide provides a simple tool for identifying genuine DNA-independent protein associations, *Proc. Natl. Acad. Sci.*, volume 89, (issue 15), August 1992, pages 6958-6962.
- [71] Banerjee, S., Tachiya, M. *et al.*, Caffeine-Mediated Detachment of Mutagenic Ethidium from Various Nanoscopic Micelles: An Ultrafast Förster Resonance Energy Transfer Study, *J. Phys. Chem. B.*, volume 116, (issue 2012), pages 7841-7848.
- [72] Shaw, A. K., Sarkar, R. *et al.*, Direct observation of DNA condensation in a nano-cage by using a molecular ruler, *Chem. Phys. Lett.*, volume 408, (issue 4-6), June 2005, pages 366-370.
- [73] Pal, S. K., Mandal, D. *et al.*, Photophysical Processes of Ethidium Bromide in Micelles and Reverse Micelles, *J. Phys. Chem. B.*, volume 102, (issue 52), December 1998, pages 11017-11023.
- [74] Tachiya, M., Application of a generating function to reaction kinetics in micelles. Kinetics of quenching of luminescent probes in micelles, *Chem. Phys. Lett.*, volume 33, (issue 2), June 1975, pages 289-292.

- [75] Infelta, P. P., Gratzel, M. *et al.*, Luminescence Decay of Hydrophobic Molecules Solubilized in Aqueous Micellar Systems. A Kinetic Model, *J. Phys. Chem.*, volume 78, (issue 2), January 1974, pages 190-195.
- [76] Tachiya, M., Kinetics of quenching of luminescent probes in micellar systems. II, *J. Chem. Phys.*, volume 76, (issue 1), 1982, pages 340-348.
- [77] Sadhu, S., Halder, K. K. *et al.*, Size Dependent Resonance Energy Transfer between Semiconductor Quantum Dots and Dye Using FRET and Kinetic Model, *J. Phys. Chem. C*, volume 114, (issue 9), February 2010, pages 3891-3897.
- [78] Gehlen, M. H., Auweraer, M. V. *et al.*, Fluorescence Quenching in Micellar Microdomains. Analysis of an Approximate Solution to the Fluorescence Decay Including Exchange of Probe and Quencher, *Langmuir*, volume 8, (issue 1), January 1992, pages 64-67.
- [79] Sarkar, R., Pal, S. K., Interaction of Hoechst 33258 and Ethidium with Histone1-DNA Condensates, *Biomacromolecules*, volume 8, (issue 11), September 2007, pages 3332-3339.
- [80] Chen, T. R., In situ detection of mycoplasma contamination in cell cultures by fluorescent Hoechst 33258 stain, *Experimental Cell Research*, volume 104, (issue 2), February 1977, pages 255-262.

### Authors' information

Department of Chemical, Biological & Macromolecular Sciences,  
S. N. Bose National Centre for Basic Sciences,  
Block JD, Sector III, Salt Lake,  
Kolkata 700 098, India.  
E-mail: [skpal@bose.res.in](mailto:skpal@bose.res.in)



**Soma Banerjee** was born (1986) in Kolkata, India. Upon accomplishing her B.Sc. (2007) and M.Sc. (2009) degrees in biochemistry, both from the Calcutta University, Kolkata (India), she joined Ph.D. under the supervision of Dr. Samir Kumar Pal at S. N. Bose National Centre for Basic Sciences, Kolkata, India. The focus of her current study is the exploration of

biomolecular recognition of medicinally important ligands including some plant alkaloids involving ultrafast spectroscopy.



**Samir Kumar Pal** (Corresponding Author) is presently associate professor in the Department of Chemical Biological and Macromolecular Sciences, S.N. Bose National Centre for Basic Sciences, Kolkata, India. He is also one of the investigators in the unit for Nano Science and Technology of the Centre.

Web: <http://www.bose.res.in/faculty/skpal.htm>